

1 **Immunotherapeutic Blockade of Macrophage Clever-1 Reactivates the**
2 **CD8⁺ T Cell Response Against Immunosuppressive Tumors**

3 Miro Viitala^{1,2}, Reetta Virtakoivu¹, Sina Tadayon^{1,2}, Jenna Rannikko¹, Sirpa Jalkanen¹, Maija
4 Hollmén^{1,*}

5 ¹MediCity Research Laboratory, Institute of Biomedicine, Faculty of Medicine, University of
6 Turku, Turku, Finland

7 ²Turku Doctoral Program of Molecular Medicine, University of Turku, Turku, Finland

8

9 *Corresponding author: Maija Hollmén, MediCity Research Laboratory, University of Turku,
10 Tykistökatu 6 A, FIN-20520, Turku, Finland. E-mail: maija.hollmen@utu.fi.

11

12 **Running title:** Clever-1 blockade activates antitumor immunity

13

14 **Financial Support:** This study was financially supported by the Sigrid Jusélius Foundation
15 (M Hollmén), the Finnish Academy (M Hollmén and S Jalkanen), the Finnish Cancer
16 Foundation (S Jalkanen), and the Finnish Cultural Foundation (R Virtakoivu).

17

18 **Disclosure of Potential Conflict of Interests:** S Jalkanen and M Hollmén own shares of
19 Faron Pharmaceuticals Ltd. (including patents also M Viitala), and are consultants for
20 Faron's CLEVEGEN program. M Hollmén reports receiving funding from Faron for the
21 preclinical development of anti-Clever-1 mAbs. No potential conflicts of interest were
22 disclosed by the other authors.

23

24 **Abbreviations:** TAM, tumor-associated macrophage; TME, tumor microenvironment;
25 BMDM, bone-marrow-derived macrophages; (PMN)-polymorphonuclear; (M)-monocytic;
26 MDSC, myeloid-derived suppressor cells

27

28 **Abstract**

29 **Purpose:** As foremost regulators of cancer-related inflammation and immunotherapeutic
30 resistance, tumor-associated macrophages have garnered major interest as immunotherapeutic
31 drug targets. However, depletory strategies have yielded little benefit in clinical studies to
32 date. An alternative approach is to exploit macrophage plasticity and “reeducate” tumorigenic
33 macrophages towards an immunostimulatory phenotype to activate the host’s antitumor
34 immunity.

35 **Experimental Design:** We investigated the role of macrophage scavenger receptor Clever-1
36 on tumor growth in multiple mouse cancer models with inflammatory and non-inflammatory
37 characteristics by using conditional knockouts, bone marrow chimeras and cell depletion
38 experiments. In addition, the efficacy of immunotherapeutic Clever-1 blockage as
39 monotherapy or in combination with anti-PD-1 was tested.

40 **Results:** Genetic deficiency of macrophage Clever-1 markedly impaired solid tumor growth.
41 This effect was mediated by macrophages that became immunostimulatory in the absence of
42 Clever-1, skewing the suppressive tumor microenvironment towards inflammation and
43 activating endogenous antitumor CD8⁺ T cells. Comparable effects were achieved with
44 immunotherapeutic blockade of Clever-1. Notably, these effects were similar to those
45 achieved by PD-1 checkpoint inhibition. Moreover, combining anti-Clever-1 with anti-PD-1
46 provided synergistic benefit in aggressive, non-responsive tumors.

47 **Conclusions:** These findings demonstrate the importance of macrophages in mediating anti-
48 tumor immune responses and support the clinical evaluation of immunotherapeutic Clever-1
49 blockade as a novel cancer treatment strategy.

50

51 **Translational Relevance:** Overcoming cancer-related immunosuppression presents a
52 significant obstacle to successful treatment. We report macrophage repolarization by
53 immunotherapeutic Clever-1 blockade as an alternative to checkpoint blockade to reactivate
54 antitumor immunity against immunosuppressive tumors.

55

56

57 **Introduction**

58 Cancer immunotherapy has proven effective for a wide range of human malignancies, but
59 solely for the minority of patients (1). Efficient and durable immunotherapies require
60 adaptive immune activation, namely antitumor CD8⁺ T cells (2). Based on immune cells
61 infiltrating the tumor microenvironment (TME), tumors have been categorized into two main
62 immunological phenotypes: inflamed tumors with spontaneous immune cell infiltration and
63 non-inflamed tumors that lack a noticeable antitumor immune response (3). Preselection of
64 patients is essential in order to achieve therapeutic outcomes, since only a minority of
65 unselected patients benefit from checkpoint blockade. For example, inhibiting PD-1/PD-L1
66 interaction in inflamed tumors can reactivate CD8⁺ T cells in the TME, sometimes leading to
67 dramatic tumor regression, whereas non-inflamed tumors are typically refractory to immune
68 checkpoint blockade (4). Still, not even all inflamed tumors respond to anti-PD-1/PD-L1
69 immunotherapies, and patients with an initial response may develop resistance. Thus, novel,
70 alternative approaches are required to reactivate antitumor immunity in a wider range of
71 patients to overcome immunotherapeutic resistance in both inflamed and non-inflamed tumor
72 types (5).

73 Macrophages are highly adaptable cells that can either stimulate or suppress the immune
74 system depending on environmental cues. Tumor-associated macrophages (TAMs) and
75 myeloid-derived suppressor cells (MDSCs) are foremost regulators of cancer-related
76 inflammation, cancer progression and immunotherapeutic resistance (6). Mirroring classical
77 M1 and alternative M2 macrophage activation, TAMs tend to acquire an M2-like tumorigenic
78 phenotype that promotes cancer progression in a multitude of ways. However, despite some
79 success in preclinical models, immunotherapies that rely on the complete depletion of TAMs
80 have not shown great success in clinical trials to date. Exploiting the inherent plasticity of
81 macrophages has been suggested as an alternative approach, and the concept of reeducating
82 tumorigenic TAMs to acquire an immunostimulatory phenotype has been proven in multiple
83 mouse models. Novel strategies for specifically depleting or converting tumorigenic TAMs
84 are therefore actively sought in immuno-oncological research (6).

85 Clever-1 (common lymphatic endothelial and vascular endothelial receptor-1) – encoded by
86 the *Stab1* gene and also called Stabilin-1 or Feel-1 – is a conserved, multifunctional adhesion
87 and scavenger receptor expressed by subsets of endothelial cells, immunosuppressive
88 macrophages and TAMs (7-11). Clever-1 mediates cell adhesion and the scavenging and
89 intracellular trafficking of its ligands (7,12-16). Recent reports by us and others indicate that

90 Clever-1 also advantages tumor progression (8-10,17). However, the proposed tumorigenic
91 mechanisms center on the paradigm of Clever-1 as an adhesion and scavenger receptor and
92 do not explain the direct immunosuppressive functions of Clever-1⁺ monocytes and
93 macrophages we have recently described (11,18,19). Mechanistic details explaining how
94 macrophage Clever-1 regulates innate–adaptive immune crosstalk and cancer-related
95 inflammation are not fully understood.

96 Here, our objective was to elucidate how macrophage Clever-1 regulates antitumor
97 immunity. We found that the growth of multiple solid tumor models is significantly impaired
98 when Clever-1 is removed specifically from macrophages. With bone marrow chimeras and
99 cell depletion experiments, we could identify macrophages deficient of Clever-1 as the
100 initiators of antitumor immunity. Lack of Clever-1 in macrophages associated with an
101 increasingly immunostimulatory phenotype and enhanced signaling through the inflammatory
102 mTOR pathway. Finally, we demonstrated that immunotherapeutic Clever-1 blockade can
103 reactivate the antitumor CD8⁺ T cell response, with comparable therapeutic responses to PD-
104 1 checkpoint blockade.

105

106 **Materials and Methods**

107 **Cell Lines**

108 The LLC1 Lewis lung carcinoma, E0771 medullary mammary adenocarcinoma and EL4
109 lymphoma cell lines were cultured in complete DMEM (Sigma-Aldrich) (DMEM
110 supplemented with 10 % FCS and penicillin/streptomycin). The 4T1-luc2 mammary gland
111 carcinoma and CT26.WT colon carcinoma were cultured in complete RPMI-1640 (Sigma-
112 Aldrich) (RPMI-1640 supplemented with 10 % FCS, 2 mM L-glutamine, 1 mM sodium
113 pyruvate and penicillin/streptomycin). The LLC1, EL4 and CT26.WT cell lines were
114 obtained from ATCC. The 4T1-luc2 cell line was obtained from Caliper Life Sciences. The
115 E0771 cell line was a generous gift from Prof. Burkhard Becher (University of Zürich,
116 Zurich, Switzerland). The cell lines were routinely tested for mycoplasma. Cell line
117 authentication was not routinely performed.

118 **Mouse Models and Therapeutic Treatments**

119 All animal experiments were performed in adherence to the Finnish Act on Animal
120 Experimentation (62/2006) and were approved by the Committee for Animal
121 Experimentation (license numbers 5587/04.10.07/2014 and 5762/04.10.07/2017). Mice were
122 used at 2–4 months of age. Experimental groups were matched for age and sex. The full and
123 conditional Clever-1 knockout mouse strains and their wildtype controls are from the
124 C57BL/6N:129SvJ mixed background and were generated as described (10). To generate
125 reporter mice, Tg(CAG-DsRed*MST)1Nagy/J mice were purchased from Jackson
126 Laboratories and crossbred with Clever-1 knockout mice to generate DsRed and
127 DsRed/Clever-1^{-/-} reporter strains. To generate LLC1, EL4 or CT26.WT tumors, 0.5×10^6
128 cells in 200 μ l of PBS were injected s.c. into the flanks. To generate orthotopic E0771 or
129 4T1-luc2 tumors, 0.1×10^6 cells in 50 μ l of PBS were injected s.c. into the fourth mammary
130 fat pads. Tumor outgrowth was measured with digital calipers. The humane endpoint for
131 tumor diameter was 15 mm. Tumor volumes were calculated as follows: longer diameter \times
132 shorter diameter² / 2. To generate bone marrow chimeras, wildtype recipients were irradiated
133 twice with 5 Gy with a three-hour interval and injected i.v. with 10×10^6 bone marrow cells
134 from DsRed or DsRed/Clever-1^{-/-} reporter mice. Mice were allowed to reconstitute for two
135 months before being used for experiments. Chimerism was determined by measuring the
136 frequency of DsRed⁺ cells in the blood. To deplete macrophages or CD8⁺ T cells, mice
137 received 200 μ g of anti-CD115 (AFS98, BioXCell) every other day or 100 μ g of anti-CD8 β

138 (53-5.8, BioXCell) once weekly, respectively, or a combination of equivalent amounts of
139 irrelevant IgGs (2A3 and HRPN, respectively, BioXCell) i.p. in PBS from eight days before
140 the cancer cell injection until endpoint. For immunotherapy, tumor-bearing mice received
141 200 µg of anti-Clever-1 (mStab1-1.26 (mouse IgG1), InVivo Biotech) (20), 200 µg of anti-
142 PD-1 (RMP1-14, BioXCell) or a combination of equivalent amounts of irrelevant IgGs
143 (MOPC-21 and 2A3, respectively, BioXCell) i.p. in PBS on days 3, 6, 9 and 12 after cancer
144 cell injection.

145 ***Ex Vivo* Bioluminescence Imaging**

146 On the day of sacrifice, mice received 150 mg/kg of D-luciferin substrate i.p. (Caliper Life
147 Sciences) and were sacrificed after 5 min by CO₂ asphyxiation. The lungs and lymph nodes
148 were excised and imaged with the IVIS system after 10 min with the following settings:
149 exposure time = 10 seconds (lungs) or 30 seconds (lymph nodes), f/stop=1, medium binning,
150 field of view = 3.9 × 3.9 cm². Living Image software was used to quantify the bioluminescent
151 signal reported as units of tissue radiance (photons/s/cm²/sr).

152 **Flow Cytometric Analysis**

153 Mice were sacrificed by CO₂ asphyxiation. Lymph nodes were dissociated mechanically.
154 Tumors were processed into single cell suspensions with the Mouse Tumor Dissociation Kit
155 per manufacturer's instructions (130-096-730, Miltenyi Biotec) and passed through 70 µm
156 pre-separation filters (130-095-823, Miltenyi Biotec). Myeloid cells and T cells were
157 enriched sequentially with CD11b and CD90.2 Microbeads, respectively (130-049-601 and
158 130-049-101, Miltenyi Biotec) on MS columns (130-042-201, Miltenyi Biotec). Cells were
159 labelled with a fixable viability dye (eFluor 450 or eFluor 780, Invitrogen) and stained with
160 conjugated primary antibodies against mouse CD3 (17A2, BD), CD4 (GK1.5, Biolegend),
161 CD8α (53-6.7, BD), CD11b (M1/70, BD), CD45 (30-F11, BD), CD206 (C068C2,
162 Biolegend), Ly6C (AL-21, Thermo Fisher), Ly6G (BD), FoxP3 (Thermo Fisher), Ki67
163 (SolA15, Thermo Fisher), Lag3 (Thermo Fisher), Nos2 (CXNFT, Thermo Fisher) and PD-1
164 (Thermo Fisher) or an irrelevant IgG control antibody with Fc block (2.4G2, BD). Anti-
165 Clever-1 (mStab1-1.26, InVivo Biotech) and its irrelevant IgG control antibody (MOPC-21,
166 Bio X Cell) were conjugated with the Alexa Fluor 647 Protein Labeling Kit (A20173,
167 Invitrogen). Cells were fixed with 4 % paraformaldehyde (sc-281692, Santa Cruz) and
168 stained in 1× Permeabilization Buffer (00-8333-56, Thermo Fisher) to detect intracellular
169 antigens (Clever-1, CD206, Nos2). The Transcription Factor Staining Buffer Set (00-5523-

170 00, Invitrogen) was used for simultaneous detection of cell-surface and intranuclear antigens
171 (Ki67, FoxP3). Samples were acquired with LSRFortessa (BD) and analysed with FlowJo 10
172 (TreeStar). Cell numbers per mg of tumor were calculated as follows: number of acquired
173 events / acquired volume \times sample volume / tumor weight.

174 **Immunohistochemistry**

175 For hematoxylin/eosin staining, 5 μ m thick tumor sections were stained with ready-to-use
176 hematoxylin (CS700), Bluing Solution (CS702) and eosin (CS701) from Dako. Briefly,
177 sections were washed with Milli-Q water, stained with hematoxylin and washed again with
178 Milli-Q water and 70 % ethanol. Next, sections were incubated with Bluing Solution, washed
179 with Milli-Q water and ethanol, stained with eosin and washed with ethanol and xylene
180 before mounting with DPX Mountant (06522, Sigma Aldrich). Samples were imaged with a
181 Panoramic 250 Slide Scanner (3D Histech Ltd.). For immunofluorescence staining, 5 μ m
182 thick tumor sections were fixed and permeabilized with acetone. Sections were stained with
183 anti-mouse CD3 (ab33429, Abcam), CD31 (550274, BD), F4/80 (53-4801-82, Thermo
184 Fisher) and Clever-1 (9-11, InVivo Biotech) or an irrelevant IgG control antibody. Sections
185 were washed with PBS and the nuclei were stained with Hoechst. Sections were mounted
186 with Vectashield Mounting Medium. Images were acquired with a Carl Zeiss LSM780 laser
187 scanning confocal microscope. The anti-Clever-1 antibody 9-11 was conjugated with the
188 Alexa Fluor 647 Protein Labeling Kit as described above.

189 **Enrichment of TAMs and MDSCs**

190 Tumors were processed into single-cell suspensions as described above. First, M-MDSCs and
191 PMN-MDSCs were enriched as one pool with the Myeloid-derived Suppressor Cell Isolation
192 Kit (130-094-538, Miltenyi Biotec), after which TAMs were enriched from the negative
193 fraction with CD11b Microbeads. The purity of enriched MDSCs was over 90 % (live
194 CD11b⁺ Ly6C^{intermediate} Gr-1⁺). The remaining CD11b fraction contained TAMs (Ly6C^{low} Gr-
195 1⁻) and some Ly6C^{high} monocytes.

196 **Generation of BMDMs**

197 Wildtype and Clever-1^{-/-} mice were sacrificed and their femurs and tibias flushed with PBS
198 using a 30G needle. Bone marrow cells were counted, resuspended to 1.0×10^6 cells/ml in
199 macrophage medium (complete IMDM supplemented with 20 ng/ml M-CSF (315-02,
200 Peprotech) and incubated in non-tissue-culture-treated plates at 37 °C for one week. Half the
201 medium was replaced with fresh macrophage medium on day 4. Differentiated BMDMs were

202 polarized with 10 nM dexamethasone for 24 h, which induced Clever-1 expression in
203 approximately 80 % of wildtype macrophages. To detach macrophages, plates were washed
204 with PBS and the cells incubated with 10 mM EDTA in PBS.

205 **Multiplex Analyses**

206 Blood from tumor-bearing mice was collected by cardiac puncture at endpoint. Serum
207 samples were collected and stored at -70°C . Pieces weighing approximately 10 mg were cut
208 from tumor edges, lysed in RIPA buffer (50 mM Tris-HCl, 150 mM NaCl, 1.0 % Triton X-
209 100, 0.5 % sodium deoxycholate, 0.1 % SDS) and stored at -70°C . Protein concentration
210 was determined with the DC Protein Assay (5000111, Bio-Rad) and 10 μg of total protein
211 was used for Multiplex. Enriched MDSCs and TAMs were plated at 0.5×10^6 cells/well in
212 complete DMEM and stimulated with 0.1 $\mu\text{g}/\text{ml}$ of LPS overnight. Supernatants were
213 collected and stored at -70°C . To normalize Multiplex readouts to cell number, the amount
214 of DNA/well was determined with the CyQuant kit (C35011, Thermo Fisher). Multiplex
215 analysis was performed with the Bio-Plex Pro Mouse Cytokine 23-plex assay (m60009rdpd,
216 BioRad) per the manufacturer's instructions. Samples were analyzed with the Bio-plex 200
217 system (BioRad).

218 **Seahorse Assays**

219 For the glycolysis stress test, enriched TAMs and MDSCs were plated at 0.1×10^6 cells/well
220 in complete IMDM and left to adhere on Seahorse Assay Plates for one hour at 37°C . IMDM
221 was replaced with Seahorse Assay Medium supplemented with 2 mM L-glutamine. The cells
222 were treated sequentially with 10 mM glucose, 1 μM oligomycin and 50 mM 2-deoxyglucose
223 and analyzed with the Seahorse XF^e96 Extracellular Flux Analyzer (Agilent Technologies).
224 For the metabolic phenotype test, wildtype and Clever-1^{-/-} BMDMs were generated as
225 described above and plated at 0.1×10^6 cells/well on Seahorse Assay Plates. IMDM was
226 replaced with Seahorse Assay Medium supplemented with 10 mM glucose, 2 mM L-
227 glutamine and 1 mM sodium pyruvate. The cells were treated with 1 μM oligomycin and
228 1 μM FCCP and analyzed as above. To normalize Seahorse Assay readouts to cell number,
229 the amount of DNA/well was determined with the CyQuant kit as above.

230 **Quantitative PCR**

231 Total RNA of dexamethasone polarized and LPS treated (50ng/ml) BMDMs were isolated
232 according to the manufacturer's instruction (NucleoSpin RNA, Macherey–Nagel). 500ng of
233 extracted RNA was used as template for the reverse transcriptase reaction made with

234 SuperScript VILO cDNA synthesis kit (ThermoFisher Scientific). Roche Universal Library
235 system was used for the quantitative PCR: 100 nM of the UPL probes, 400 nM of the primers
236 (Stabilin1: CTGTGTCCTGGTCCTCTGC and CGCAACGTTTAGACCGTACC, β -Actin:
237 CTAAGGCCAACCGTGAAAAG and ACCAGAGGCATACAGGGACA) and 5 ng of
238 cDNA was used per well and three technical replicates were made. Reactions were ran with
239 QuantStudio 12K Flex Real-Time PCR System (Applied Biosystems/ ThermoFisher
240 Scientific) at the Finnish Microarray and Sequencing Centre (FMSC), Turku Centre for
241 Biotechnology, Turku, Finland. Relative expression of Stabilin1 was calculated by using S
242 equence Detection System (SDS) Software v2.4.1, QuantStudio 12 K Flex software and
243 DataAssist software (Applied Biosystems/ThermoFisher Scientific). β -Actin was used as an
244 endogenous control.

245 **Western Blotting**

246 Dexamethasone-polarized wildtype and Clever-1^{-/-} BMDMs were stimulated with 50 ng/ml
247 LPS for various time points and lysed with Triton X-100 lysis buffer (2 % Triton X-100,
248 10 mM Tris-HCl, 150 mM NaCl, 1.5 mM MgCl₂, 1 mM PMSF, EDTA-free protease
249 inhibitor cocktail). Protein concentration was measured with the Bradford method and equal
250 amounts of protein (8–12 μ g depending on the experiment) were loaded into 4–20 % Mini-
251 PROTEAN Precast Protein Gels (4561094, Bio-Rad). Separated proteins were transferred to
252 membranes using a Trans-Blot Turbo Mini Nitrocellulose Transfer Pack (1704158, Bio-Rad).
253 Membranes were incubated with primary antibodies against mouse p-mTOR S2248 (109368,
254 Abcam), p-NF- κ B S536 (3033S, Cell Signaling Technology) and GAPDH (5G4, Hytest
255 Ltd.). IRDye 680RD donkey anti-mouse (C70419-09, LI-COR) and IRDye 800CW donkey
256 anti-rabbit (C70918-02, LI-COR) were used as secondary antibodies. Fluorescence signal
257 was detected with the Odyssey LI-COR Imaging System. Image analysis and band
258 quantification were performed with ImageJ.

259 **Statistical Analyses**

260 Data are presented as mean \pm SEM with bar graphs additionally showing individual data
261 points. Comparisons between groups were performed with the Mann-Whitney *U* test or the
262 Kruskal-Wallis test followed by Mann-Whitney *U* tests. Comparisons between growth curves
263 were performed with repeated measures two-way ANOVA followed by Tukey's multiple
264 comparisons tests. *P* < 0.05 was considered statistically significant. Statistical analyses were
265 performed with Prism 7 (GraphPad).

266 **Results**

267 **Macrophagic Clever-1 Deficiency Significantly Impairs Tumor Growth**

268 To dissect the contribution of macrophage Clever-1 on the progression of solid tumors, we
269 studied the outgrowth of subcutaneous LLC1 Lewis lung adenocarcinoma over two weeks in
270 syngeneic wildtype, full Clever-1 knockout (Clever-1^{-/-}) and macrophage Clever-1 knockout
271 (*Lyz2-Cre/Clever-1^{fl/fl}*) mice (10). The tumors grew comparably for the first week, after
272 which tumor outgrowth was significantly impaired in Clever-1^{-/-} and especially in *Lyz2-*
273 *Cre/Clever-1^{fl/fl}* mice (**Fig. 1A and B**; Supplementary Fig. 1A). Similarly, tumor weights
274 were reduced in both Clever-1^{-/-} and even more so in *Lyz2-Cre/Clever-1^{fl/fl}* mice on day 15
275 (**Fig. 1C**). The increased tumor control in *Lyz2-Cre/Clever-1^{fl/fl}* mice was also reflected in the
276 substantial reduction of serum G-CSF, a cytokine produced by LLC1 tumors (**Fig. 1D**) (21).
277 Additionally, tumors in both Clever-1^{-/-} and *Lyz2-Cre/Clever-1^{fl/fl}* mice contained
278 significantly fewer non-hematopoietic tumor cells (gated on live CD45⁻ cells) (**Fig. 1E** and
279 Supplementary Fig. 1B) with increased PD-L1 expression (**Fig. 1F**), suggesting that
280 immunoediting of the surviving tumor cells occurred over the two-week period. No
281 significant difference was observed in the proliferation of tumor cells (Ki67⁺) or the number
282 of CD31⁺ vascular endothelial cells on day 15 (Supplementary Fig. 1C).

283 As additional syngeneic cancer models, we studied the outgrowth of orthotopic E0771
284 medullary mammary adenocarcinoma and subcutaneous EL4 lymphoma in wildtype, Clever-
285 1^{-/-} and *Lyz2-Cre/Clever-1^{fl/fl}* mice (**Fig. 1G and H**). Strikingly, the outgrowth of both E0771
286 and EL4 tumors was significantly impaired in *Lyz2-Cre/Clever-1^{fl/fl}* mice, with all E0771
287 tumors cleared by day 15. However, neither cancer model showed clear reduction in tumor
288 growth in Clever-1^{-/-} mice (**Fig. 1G and H**). Still, the frequency of PD-L1⁺ non-
289 hematopoietic cells had increased also in E0771 tumors grown in Clever-1^{-/-} mice
290 (Supplementary Fig. 1D). Additionally, the outgrowth of EL4 tumors was not impaired at all
291 in *Tie2-Cre/Clever-1^{fl/fl}* mice, where Clever-1 is deleted from the vascular endothelium (**Fig.**
292 **1H**), although anti-Clever-1 treatment of wild type mice bearing EL-4 tumors results in
293 diminished size of primary tumors and metastases (10). Together, these results demonstrate
294 that Clever-1 deficiency can significantly impair the progression of multiple syngeneic
295 models of solid cancers. Furthermore, they suggest that the improved tumor control is
296 mediated by macrophages but not by vascular endothelial cells deficient of Clever-1.

297 **Clever-1-Deficient Mice Can Overcome Cancer-Related Immunosuppression**

298 LLC1 tumors are poorly immunogenic and induce general T cell exhaustion, thus inhibiting
299 antitumor immunity (22). To explore how Clever-1 deficiency affected the ongoing systemic
300 immune responses in tumor-bearing wildtype, Clever-1^{-/-} and *Lyz2-Cre/Clever-1^{fl/fl}* mice, we
301 analyzed serum cytokine levels on day 15. We found elevated levels of the key inflammatory
302 cytokines IL-1 β , IL-2, IL-12p70 and TNF- α as well as the inflammatory chemokines CCL3,
303 CCL4 and CCL5 in Clever-1^{-/-} mice, but surprisingly not so in *Lyz2-Cre/Clever-1^{fl/fl}* mice
304 (**Fig. 2A and B**). The lack of elevated cytokine levels in the serum of *Lyz2-Cre/Clever-1^{fl/fl}*
305 mice was probably consequent to their advanced tumor control. The observed increase in
306 cytokines was tumor related since no differences were seen in non-tumor bearing mice
307 between the genotypes apart from significantly higher IL-1 β in Clever-1^{-/-} mice (data not
308 shown).

309 We then investigated how Clever-1 deficiency affected adaptive immune activation in the
310 TME. Immunofluorescence imaging of tumors collected from *Lyz2-Cre/Clever-1^{fl/fl}* mice
311 revealed massive infiltration of CD3⁺ lymphocytes that were confirmed as CD8⁺ T cells by
312 flow cytometric analysis (pre-gated on live CD45⁺ CD3⁺ cells), although no significant
313 differences in tumor-infiltrating lymphocytes were observed between tumors from wildtype
314 and Clever-1^{-/-} mice (**Fig. 2C and D**; Supplementary Fig. 2A). The amount of T_{reg} (CD4⁺
315 FoxP3⁺) and CD4⁺ T cells (CD4⁺ FoxP3⁻) were comparable between the genotypes (**Fig.**
316 **2D**). Still, the prognostic CD4⁺/CD8⁺ ratio decreased significantly in both Clever-1^{-/-} and
317 *Lyz2-Cre/Clever-1^{fl/fl}* mice (**Fig. 2E**). Moreover, the CD8⁺ T cells in tumors from both
318 Clever-1^{-/-} and *Lyz2-Cre/Clever-1^{fl/fl}* mice showed significantly increased co-expression of
319 the exhaustion markers Lag3 and PD-1 (**Fig. 2F**) as did the CD4⁺ T cells (Supplementary Fig.
320 2B), indicating robust and prolonged T cell activation (23). Additionally, we observed
321 increased frequencies of proliferating CD8⁺ effector T cells in the tumor-draining lymph
322 nodes of Clever-1^{-/-} and *Lyz2-Cre/Clever-1^{fl/fl}* mice (**Fig. 2G**), suggesting that Clever-1
323 deficiency led to the increased priming of antitumor CD8⁺ T cells outside the tumor.

324 **Macrophages and CD8⁺ T Cells Are Required for Tumor Control in Clever-1-Deficient** 325 **Mice**

326 To validate that the strikingly improved tumor control in *Lyz2-Cre/Clever-1^{fl/fl}* mice was not
327 a non-specific effect due to, for example, the Cre recombinase expressed under the *Lyz2*
328 promoter, we bred DsRed and DsRed/Clever-1^{-/-} reporter mice and used them to create bone

329 marrow chimeras to imitate the *Lyz2-Cre/Clever-1^{fl/fl}* phenotype (**Fig. 3A**). Briefly, irradiated
330 wildtype recipients were intravenously injected with bone marrow from DsRed or
331 DsRed/*Clever-1^{-/-}* donors and allowed to reconstitute for two months. Following
332 reconstitution, we studied the outgrowth of LLC1 tumors in the resulting wildtype→wildtype
333 and *Clever-1^{-/-}*→wildtype chimeras. Remarkably, tumor outgrowth was significantly
334 impaired in the *Clever-1^{-/-}*→wildtype chimeras (**Fig. 3B**), with a concomitant increase in
335 tumor-infiltrating CD8⁺ T cells comparable to that observed in *Lyz2-Cre/Clever-1^{fl/fl}* mice
336 (**Fig. 3C and D**). TAMs in *Clever-1^{-/-}*→wildtype chimeras lacked *Clever-1* expression and
337 were decreased in frequency (**Fig. 3C, E and F**). Furthermore, TAMs in *Clever-*
338 *1^{-/-}*→wildtype chimeras expressed more MHC II and less CD206 (**Fig. 3G and H**), an
339 established marker for M2 macrophages. These results suggest that in the absence of
340 macrophage *Clever-1*, TAMs acquire an immunostimulatory phenotype, which associates
341 with increased tumor infiltration by CD8⁺ T cells.

342 We then wanted to corroborate that macrophages are required to initiate tumor control in
343 *Lyz2-Cre/Clever-1^{fl/fl}* mice and to verify that this tumor control is executed by CD8⁺ T cells.
344 To this end, we depleted macrophages or CD8⁺ T cells from wildtype and *Lyz2-Cre/Clever-*
345 *1^{fl/fl}* mice with antibodies against CD115 or CD8β, respectively, and measured the outgrowth
346 of LLC1 tumors (**Fig. 3I and J**). Remarkably, depleting either macrophages or CD8⁺ T cells
347 reversed the efficient tumor control seen in *Lyz2-Cre/Clever-1^{fl/fl}* mice (**Fig. 3J**),
348 demonstrating that *Clever-1*-deficient macrophages, in conjunction with CD8⁺ T cells, are
349 required to establish an efficient antitumor response. Flow cytometric analysis showed
350 substantial depletion of TAMs and CD8⁺ T cells from the TME at endpoint (**Fig. 3K**). Taken
351 together, *Clever-1* deficient macrophages are essential for initiating CD8⁺ T cell mediated
352 tumor control.

353 **Clever-1 Deficiency Increases the Immunostimulatory Activity of Tumor-Associated** 354 **Macrophages**

355 Our previous studies on the B16 mouse melanoma model suggested that much of the
356 antitumor effect of *Clever-1* deficiency would be mediated by the tumor endothelium (10).
357 However, with the LLC1 lung cancer model, the improved tumor control in *Clever-1-*
358 *deficient* mice became discernible approximately one week after cancer cell injection, at
359 which point LLC1 tumors lacked *Clever-1* expression on the endothelium but contained a
360 high frequency of *Clever-1⁺* TAMs (**Fig. 4A**). At steady state the frequency and distribution
361 of macrophages (CD11b⁺F4/80⁺) in the blood, bone marrow, lungs, peripheral lymph nodes,

362 and spleen of wildtype and *Cleaver-1*^{-/-} mice was somewhat similar as we only observed
363 roughly a 5% increase in bone marrow and a 5% decrease in blood macrophages in *Cleaver-1*^{-/-}
364 mice compared to wildtype mice (Supplementary Fig 3A). By day 15, nearly all of the
365 tumor endothelial cells were *Cleaver-1*⁺ (pre-gated on live CD45⁻ CD31⁺ cells), but little
366 *Cleaver-1* expression could be detected on CD45⁻ CD31⁻ tumor cells or CD45⁺ CD11b⁺
367 myeloid cells in the spleen or tumor-draining lymph nodes (Supplementary Fig. 3B). To
368 investigate how *Cleaver-1* deficiency could result in such efficient immune activation and
369 tumor control, we analyzed the composition of the main myeloid cell populations (pre-gated
370 on live CD11b⁺ cells) found in tumors (**Fig. 4B**). While the number of polymorphonuclear
371 (PMN)-MDSCs (Ly6C^{intermediate} Ly6G⁺) and monocytic (M)-MDSCs (Ly6C^{high} Ly6G⁻) in
372 LLC1 tumors were comparable between the genotypes, the number of TAMs (Ly6C^{low}
373 Ly6G⁻) (pre-gated on live CD11b⁺ cells; Supplementary Fig. 3C) were significantly reduced
374 in *Cleaver-1*^{-/-} mice and nearly absent from *Ly2z-Cre/Cleaver-1*^{fl/fl} mice (**Fig. 4B**). On day 15,
375 on average 30 % of TAMs were *Cleaver-1*⁺, and TAMs were the only myeloid cell population
376 in tumors to express *Cleaver-1* (**Fig. 4C**; Supplementary Fig. 3D). The majority of TAMs are
377 the progeny of M-MDSCs that infiltrate the TME and polarize in response to environmental
378 cues. Although tumors in *Cleaver-1*^{-/-} mice contained fewer TAMs, M-MDSCs in tumors
379 from *Cleaver-1*^{-/-} mice actually expressed more Ki67 (Supplementary Fig. 3E), implying that
380 the decrease in TAMs was not due to decreased M-MDSC infiltration or proliferation.

381 Although, the number of total TAMs decreased in *Cleaver-1*^{-/-} mice, the frequency of MHC
382 II^{high} TAMs increased in tumors from *Cleaver-1*^{-/-} mice (**Fig. 4D**). Intriguingly, the MHC II^{high}
383 TAMs in *Cleaver-1*^{-/-} mice co-expressed higher levels of CD206 (**Fig. 4E**). A similar
384 phenotypic alteration was observed in TAMs from E0771 tumors collected from *Cleaver-1*^{-/-}
385 mice (Supplementary Fig. 3F). These differences were not due to increased numbers of
386 dendritic cells, as tumors from *Cleaver-1*^{-/-} mice actually contained fewer CD11c⁺ MHC II^{high}
387 cells (pre-gated on live cells) (Supplementary Fig. 4A and B). Furthermore, TAMs from
388 *Cleaver-1*^{-/-} mice expressed less PD-L1 (**Fig. 4F**) and showed defective upregulation of
389 inducible nitric oxide synthase (*Nos2*) after LPS stimulation *ex vivo* (**Fig. 4G**), while in
390 PMN- and M-MDSCs, *Nos2* expression was unaltered (Supplementary Fig. 5B).
391 Additionally, direct Multiplex analysis of tumor lysates showed increased IL-12p40 in tumors
392 from *Cleaver-1*^{-/-} mice (**Fig. 4H**). Increased secretion of IL-12p40 was detected also from the
393 supernatants of enriched TAMs stimulated with LPS overnight (**Fig. 4I**), but not from MDSC

394 supernatants (Supplementary Fig. 5A and C). Due to their scarcity, similar analyses could not
395 be performed on TAMs from *Lyz2-Cre/Clever-1^{fl/fl}* mice.

396 **The Increasingly Inflammatory Phenotype of Clever-1-deficient Macrophages** 397 **Associates with Increased mTOR Activity**

398 The immunostimulatory activation in TAMs associates with a metabolic switch from
399 oxidative phosphorylation to glycolysis (24). To analyze metabolic differences between
400 TAMs from wildtype and *Clever-1^{-/-}* mice, we performed the Seahorse glucose stress test on
401 enriched TAMs and observed increased glycolysis and glycolytic capacity (ECAR,
402 extracellular acidification rate) in TAMs enriched from *Clever-1^{-/-}* mice (**Fig. 5A and B**),
403 while no difference in glycolytic activity was observed between MDSCs (Supplementary Fig.
404 5D and E). Typically, classically activated macrophages upregulate glycolytic pathways in
405 response to increased mTOR activity (25). Thus, we investigated whether *Clever-1*
406 deficiency alters the activity of this inflammatory signaling pathway in bone-marrow-derived
407 macrophages (BMDM) derived from wildtype or *Clever-1^{-/-}* mice. BMDMs were polarized
408 with dexamethasone for 24 h to induce robust *Clever-1* expression (Supplementary Fig. 6A
409 and B). In line with previous reports, *Clever-1* deficiency did not inhibit macrophage
410 differentiation *in vitro* (Supplementary Fig 6C). However, flow cytometric analysis of
411 dexamethasone-polarized BMDMs revealed a significant increase in the frequency of
412 CD206⁺ MHC II⁺ double-positive cells in *Clever-1^{-/-}* BMDM cultures (**Fig. 5C**), reflecting
413 the phenotype of TAMs in *Clever-1^{-/-}* mice. Additionally, *Clever-1^{-/-}* BMDMs expressed
414 less PD-L1 on the cell surface (**Fig. 5D**) and secreted less IL-10 after LPS stimulation (**Fig.**
415 **5E**).

416 Similar to *Clever-1^{-/-}* TAMs, the dexamethasone polarized *Clever-1^{-/-}* BMDMs showed
417 increased glycolysis but not oxidative phosphorylation (OCR, oxygen consumption rate) at
418 baseline (**Fig. 5F and G**). After overnight LPS stimulation, no differences were observed in
419 the metabolic activity between wildtype and *Clever-1^{-/-}* BMDMs (**Fig. 5F and G**). This was
420 likely due to the rapid downregulation of *Clever-1* mRNA in response to LPS (**Fig. 5H**).
421 When the immediate responses to LPS stimulation were measured, *Clever-1^{-/-}* BMDMs
422 showed a rapid and prolonged increase in mTOR phosphorylation (**Fig. 5I and J**), which was
423 corroborated also by flow cytometry (**Fig. 5K**) suggesting that metabolic remodeling was
424 more efficient in the absence of *Clever-1*.

425 **Immunotherapeutic Clever-1 Blockade Significantly Impairs Solid Tumor Growth**

426 Previously, we have reported that immunotherapeutic Clever-1 blockade with the mStab1-
427 1.26 antibody attenuates tumor growth in the B16 mouse melanoma model (10). To compare
428 the effects of anti-Clever-1 treatment to an immunotherapeutic treatment mainly targeting the
429 adaptive immune response, we treated mice bearing established LLC1 tumors with the anti-
430 PD-1 antibody RMP1-14 (26) as monotherapy or in combination with anti-Clever-1 (**Fig.**
431 **6A**). All three treatments clearly reduced the size and weight of tumors compared to the
432 irrelevant IgG treatment (**Fig. 6B–D**). Notably, tumors from mice treated with anti-Clever-1
433 were even smaller than those treated with anti-PD-1, although the difference between the
434 groups was not statistically significant. The combination treatment did not bring additional
435 benefit to the monotherapies in the LLC1 model, and was accompanied by impaired
436 clearance of non-hematopoietic tumor cells (**Fig. 6E**). To gain further insight into the
437 mechanisms of tumor rejection mediated by Clever-1 interference, the treatment regimens
438 were repeated with the metastasizing 4T1-luc2 breast cancer and immunogenic CT26.WT
439 colon carcinoma models (27). The combination of anti-Clever-1 and anti-PD-1 was most
440 effective at inhibiting 4T1-luc2 tumor growth, viability and metastasis to the lungs and
441 tumor-draining lymph nodes (Supplementary Fig. 7A–D). Also, in the CT26.WT model the
442 combination treatment brought slightly more effect compared to anti-PD-1 alone
443 (Supplementary Fig. 7E–G). Interestingly, only anti-Clever-1 treatment led to a decrease in
444 the frequencies of PD-L1⁺ non-hematopoietic tumor cells in the immunologically cold LLC1
445 model (**Fig. 6F**), suggesting that anti-PD-1 treatment induces immunotherapeutic resistance
446 mediated by the upregulation of PD-L1, but that this mechanism may not be protective
447 against Clever-1 blockade alone. Conversely, in the immunologically hot CT26.WT model,
448 wherein a much higher frequency of tumor cells were PD-L1⁺ to start with, the combinatorial
449 treatment most successfully decreased the frequencies of PD-L1⁺ tumor cells (Supplementary
450 Fig. 7H).

451 **Clever-1 Antibody Blockade Reactivates the Antitumor CD8⁺ T Cell Response**

452 When analyzing the adaptive immune response, we did not observe any significant
453 differences in the numbers of tumor-infiltrating CD4⁺ T cells or T_{reg} cells between the
454 treatments (**Fig. 6G**). Surprisingly, however, we observed that the numbers of CD8⁺ T cells
455 were actually decreased in LLC1 tumors treated with anti-Clever-1 alone (**Fig. 6G**), but the
456 frequencies of tumor-infiltrating CD4⁺ effector T cells (CD44^{high} CD62L^{low}) and CD8⁺
457 memory T cells (CD44^{high} CD62L^{high}) were significantly increased in tumors treated with

458 anti-Clever-1, even more so compared to Clever-1^{-/-} mice (Supplementary Fig. 8A and B).
459 Furthermore, the numbers of CD8⁺ T cells were unchanged in tumors treated with anti-PD-1
460 alone and significantly increased in tumors treated with the combination (**Fig. 6G**). Despite
461 these differences, all three treatments increased the frequencies of proliferating PD-1⁻ CD8⁺
462 T cells (**Fig. 6H**), implicating that both anti-Clever-1 and anti-PD-1 treatment can reactivate
463 antitumor CD8⁺ T cells and that these treatments can work synergistically in this regard.
464 Interestingly, while the total TAM and PMN-MDSC populations were greatly reduced by
465 anti-Clever-1 and anti-PD-1 treatments alone, their combination normalized the distribution
466 of tumor-associated myeloid cells to that of irrelevant IgG treatment (**Fig. 6I**), thus perhaps
467 explaining the impairment in tumor cell clearance. The frequencies of Clever-1⁺ TAMs
468 remained unaltered in all three treatments (**Fig. 6J**), suggesting that the observed effects were
469 not caused by the depletion of Clever-1⁺ TAMs. Surface staining with the directly-conjugated
470 mStab1-1.26 antibody showed that virtually all Clever-1 on TAMs was occupied following
471 antibody treatment (Supplementary Fig. 8C). Curiously, in CT26.WT tumors, only anti-PD-1
472 treatment increased the numbers of CD8⁺ T cells and the frequencies of proliferating PD-1⁻
473 CD8⁺ T cells, while the combination with anti-Clever-1 and anti-PD-1 retained their levels
474 comparable to those of the irrelevant IgG treatment (Supplementary Fig. 7I and J). In
475 CT26.WT tumors, anti-Clever-1 treatment alone significantly reduced the numbers of both
476 M-MDSCs and TAMs, while the treatment with anti-PD-1 significantly reduced the numbers
477 of TAMs (Supplementary Fig. 7K). Although, the combination of anti-Clever-1 and anti-PD-
478 1 somewhat normalized the distribution of tumor-associated myeloid cells in CT26.WT
479 tumors similarly to what was observed in the LLC1 tumors, the numbers of TAMs remained
480 significantly reduced in comparison to the irrelevant IgG treatment (Supplementary Fig. 7K).
481 In addition, it resulted in a slight reduction in Clever-1⁺ TAMs (Supplementary Fig. 7L).
482 Taken together, these results demonstrate that anti-Clever-1 treatment results in similar
483 adaptive immune activation in the TME as genetic Clever-1 deficiency, and that these effects
484 are comparable to what can be achieved with PD-1 checkpoint blockade.

485

486 **Discussion**

487 Due to the recent successes but emerging shortcomings in immunotherapy, novel treatment
488 strategies that activate the antitumor immune response are a topic of major interest in cancer
489 immunology research. In this study, we show a significant function of the scavenger receptor
490 Clever-1 in controlling macrophage-mediated local and systemic antitumor immune
491 responses. Our data support Clever-1 targeting as a novel approach to increase host defense
492 against immunocompromised tumors alongside PD-1 blockade. Exceptionally, the improved
493 tumor control in our study was achieved by targeting the innate arm of immunity, which
494 undoubtedly underlines the importance of macrophages in controlling the fate of tumor-
495 reactive T cells. This is also supported by the notion that macrophage-targeted approaches are
496 needed to achieve full immunotherapeutic efficacy (28,29). Importantly, Advani et al. report
497 substantial anti-tumor responses in non-Hodgkin's lymphoma by blocking the CD47-SIRP α
498 checkpoint together with anti-CD20 suggesting that macrophage-mediated antibody-
499 dependent tumor cell phagocytosis can be complementary to activating T-cell-mediated
500 tumor killing (30,31).

501 Recent studies highlight the importance of DCs in the activation of antitumor immunity (32-
502 34). Although DCs are reportedly more efficient at T cell priming than TAMs, macrophages
503 can also prime CD8⁺ T cells to generate cytotoxic effector cells and CD8⁺ T cell memory *in*
504 *vivo* (32,35). Moreover, tumorigenic TAMs are extremely potent immunosuppressors both
505 individually and through sheer numbers (32,36,37). For example, tumor-infiltrating CD8⁺ T
506 cells mostly come into contact with TAMs because of their high frequency, and TAMs can
507 directly induce CD8⁺ T cell apoptosis and physically restrict CD8⁺ T cells from reaching their
508 target cells (32,38,39).

509 Paradoxically, complete TAM depletion with CSF-1R inhibition has not yielded therapeutic
510 benefits as monotherapy, and more effective responses have been reached by combining it
511 with chemotherapy, adoptive cell transfer or checkpoint blockade (40-43). In comparison,
512 monotherapies aimed at repolarizing TAMs have presented more promising results (44-46).
513 A possible reason for this is that some TAM populations susceptible to CSF-1R depletion are
514 needed for efficient antitumor control. This is in line with our data showing that the effective
515 tumor control gained by blocking Clever-1 on TAMs is fully abolished by CSF-1R treatment.
516 It is interesting to note that while Clever-1 is used as a common marker for alternatively
517 activated macrophages, it is only expressed by 20 to 40% of TAMs in various mouse tumor
518 models. Despite their relatively low numbers, our data suggest that Clever-1 expression

519 defines a subpopulation of TAMs capable of limiting effective antitumor immune responses.
520 In fact, blocking Clever-1 skewed TAMs towards an immunostimulatory phenotype with
521 increased MHC II expression and IL-12p40 secretion, thus enabling efficient antigen
522 presentation and improving tumor control by boosting infiltration of CD8⁺ T cells,
523 respectively (47). Similarly, Clever-1 knockdown in human monocytes increases their ability
524 to reactivate T cells in antigen recall assays (11). Intriguingly, the aforementioned changes
525 were accompanied by increased CD206 expression by MHC II^{high} TAMs. While CD206 is an
526 established marker for alternatively activated macrophages and mostly associated with a
527 negative impact on tumor control, macrophages have been shown to use CD206 for
528 endocytosing soluble antigens for cross-presentation and CD8⁺ T cell activation (48,49). We
529 did not observe a similar mixed TAM phenotype in the Clever-1^{-/-} bone marrow chimeras,
530 indicating that compensatory mechanisms contributing to the loss of Clever-1 on endothelial
531 cells might have induced CD206 expression on MHC II^{high} TAMs. Similarly, the PD-L1
532 induction on cancer cells in the conditional and full knockout mice was not recapitulated after
533 immunotherapeutic Clever-1 blockade, again pointing to compensatory mechanisms that
534 might have developed during the lifespan of these mice.

535 On the other hand, the induction of Nos2 was impaired in Clever-1^{-/-} TAMs in response to
536 *ex vivo* LPS stimulation. As Nos2 is greatly induced by classical activation (50), our
537 observations were not in line with a general view of the functional traits seen in classically
538 activated macrophages, *per se*. However, the TME contains multitudes of danger-associated
539 molecular patterns that can prime and activate TAMs. We can speculate that differences in
540 the composition of the TME, created either by active tumor lysis or the impaired scavenging
541 of extracellular matrix components due to the loss of Clever-1, modify the secondary
542 responses of TAMs to nonrelated stimuli, in this case to LPS. Along these lines, human
543 monocytes primed with β -glucan downregulate ROS production when re-stimulated with
544 LPS but upregulate it when primed with either the bacillus Calmette-Guérin (BCG) vaccine
545 or oxidized low-density lipoprotein (oxLDL) (51). Overall, excessive nitric oxide production
546 by Nos2 has been shown to suppress classical activation, interfere with antigen recognition
547 and induce T cell apoptosis (38,52-54).

548 The priming of macrophages induces a metabolic switch from oxidative phosphorylation to
549 glycolysis. Consistent with the priming hypothesis, Clever-1^{-/-} TAMs demonstrated
550 increased glycolysis suggesting that effective priming had occurred within the TME of LLC1
551 tumors in the absence of Clever-1. The mTOR signaling network orchestrates a multitude of

552 cellular and metabolic activities that shape immune effector responses. In mice, increased
553 mTORC1 activity and reduced mTORC2 activity by ablation of *Tsc1* has been shown to
554 promote M1 macrophage polarization (25). The increased glycolysis in *Cleaver-1*^{-/-} TAMs
555 was in line with the observed increase in phosphorylation of mTOR in *Cleaver-1*^{-/-} BMDMs
556 after LPS stimulation. Since the mTOR complex is localized within endosomes, it can be
557 speculated that mechanistically *Cleaver-1* attenuates mTOR activity by regulating its
558 endosomal trafficking. In support of this, the intracellular part of *Cleaver-1* contains a GGA-
559 binding site that is required for intracellular sorting of its ligands (55). Furthermore, a recent
560 report shows that the adaptation of metabolism after LPS stimulation in macrophages mainly
561 occurs through proteome remodeling at the translational level (56), and therefore might
562 explain why *Cleaver-1* deficiency has not been reported to induce major transcriptional
563 changes in TAMs (17).

564 One apparent difference was seen in the impaired ability of *Cleaver-1* full knockout mice to
565 mount equally effective tumor rejection in comparison to mice lacking *Cleaver-1* expression
566 only on macrophages, despite similar but milder antitumor responses. Most likely the reason
567 can be attributed to the endothelial *Cleaver-1*, which has been reported to mediate immune cell
568 adhesion to the tumor endothelium (10) as well as support immune and cancer cell migration
569 through blood and lymphatic vessels (12,14,16,57-59). As we detected here, *Cleaver-1* is
570 induced in TAMs earlier than on the tumor endothelium and increased infiltration of T cells
571 in tumors occurred before endothelial *Cleaver-1* expression. Although the kinetics of *Cleaver-1*
572 expression may differ between cancer models, it is possible that tumor endothelial *Cleaver-1* is
573 required to maintain CD8⁺ T cell infiltration at later time points. Also, the contribution of
574 lymphatic endothelial *Cleaver-1* to immune responses remains to be clarified, as it may
575 facilitate cell migration through lymph vessels into the tumor-draining lymph nodes.
576 Therefore, we believe that the loss of *Cleaver-1* on lymphatic or vascular endothelium in
577 *Cleaver-1*^{-/-} mice impairs the infiltration of activated lymphocyte subsets in the TME and
578 therefore counteracts to the pro-inflammatory effects produced by *Cleaver-1* deficient TAMs
579 in the *Lyz2-Cre/Cleaver-1*^{fl/fl} mice (Supplementary Fig 8D).

580 The anti-tumor effects obtained by immunotherapeutic *Cleaver-1* blockage with the mStab1
581 antibody were paradoxically more similar to the *Lyz2-Cre/Cleaver-1*^{fl/fl} mice than the *Cleaver-1*^{-/-}
582 mice. Since *Cleaver-1* is a very large scavenger receptor (~280 kDa), and has several
583 functional binding sites for its ligands, the binding of mStab1 on *Cleaver-1* may not fully
584 block the amino acid residues that lymphocytes use for their adhesion to the tumor

585 endothelium but sufficiently block macrophage scavenging. Rantakari et al. demonstrate that
586 the human Clever-1 antibody 3-372 can revert LDL scavenging related suppression of CCL3
587 secretion by human monocytes (19). We observed a similar increase in CCL3 secretion in
588 mStab1 treated mouse macrophages after (data not shown), and therefore believe that
589 macrophage conversion is achieved with the mStab1 antibody. Intriguingly, our unpublished
590 observations (Tadayon et al., resubmitted after revisions) indicate that Clever-1 can bind to
591 the surface of both B and CD8 T cells suggesting that Clever-1 could inhibit these cells
592 directly by an unknown ligand, and complement to the immunosuppressive nature it has on
593 TAMs.

594 Importantly, immunotherapeutic Clever-1 blockade showed a significant therapeutic effect in
595 LLC1 tumors, which was comparable or even slightly more robust than the effect seen with
596 anti-PD-1. Both of these immunotherapies altered tumor-infiltrating immune cell populations
597 in a similar manner, resulting in decreased numbers of TAMs and PMN-MDSCs and
598 increased frequencies of activated CD8⁺ T cells. The lower abundance of TAMs and PMN-
599 MDSCs can partially explain the therapeutic effect. However, the frequency of Clever-1⁺
600 TAMs did not change after anti-Clever-1 treatment, suggesting that the effect does not come
601 from the depletion of Clever-1⁺ cells due to antibody-dependent cell cytotoxicity. Curiously,
602 the numbers of total CD8⁺ T cells were decreased by anti-Clever-1 treatment. This may be a
603 result of endothelial Clever-1 blockade, as the numbers of total CD8⁺ T cells were not
604 increased in Clever-1^{-/-} mice, either. A noteworthy dissimilarity between anti-Clever-1 and
605 anti-PD-1 treatments was the downregulation of PD-L1 on non-immune tumor cells after
606 treatment with anti-Clever-1 but not anti-PD-1. This suggests that upregulation of the PD-L1
607 checkpoint, a common mechanism of immunotherapeutic resistance, is not protective against
608 anti-Clever-1 treatment, or that alternative resistance mechanisms are activated by anti-
609 Clever-1 treatment.

610 The therapeutic effect of anti-Clever-1 treatment in different tumor types might not be
611 directly reflected to the number of Clever-1⁺ TAMs in the TME. The immunologically cold
612 LLC1 tumors contained half the number of Clever-1⁺ TAMs compared to the CT26.WT
613 tumors and yet produced much higher response rates as monotherapy. One possible reason
614 for this is the high expression of PD-L1 on CT26.WT cells that was not downregulated by
615 anti-Clever-1 monotherapy in a similar fashion as seen in LLC1 tumors. Lack of PD-L1
616 expression on malignant cells has been shown to delay tumor growth in a CD8⁺ T cell
617 mediated fashion (60). Thus, despite higher numbers of CD8⁺ T cells in the combination

618 treated LLC1 tumors, consistent PD-L1 expression on LLC1 cells might have rendered this
619 combination ineffective. On the other hand, the combination treatment in the CT26.WT
620 model significantly suppressed PD-L1 expression on the tumor cells and produced a modest
621 synergistic effect compared to anti-PD-1 alone.

622 Taken together, we propose that the improved tumor control is specifically a result of
623 macrophage Clever-1 deficiency, which increases the frequency of immunostimulatory
624 TAMs while reducing their total numbers, together rendering the TME more permissive to
625 CD8⁺ T cell activation. Additionally, we show that immunotherapeutic anti-Clever-1
626 treatment can achieve comparable outcomes to PD-1 checkpoint blockade strongly
627 supporting the clinical evaluation of Clever-1 targeting as a novel cancer treatment strategy.

628

629 **Author's Contributions**

630 **Conception and design:** M Viitala, M Hollmén

631 **Development of methodology:** M Viitala, R Virtakoivu, S Tadayon, M Hollmén

632 **Acquisition of data (provided animals, provided facilities, etc.):** M Viitala, R Virtakoivu,
633 S Tadayon, J Rannikko, S Jalkanen, M Hollmén

634 **Analysis and interpretation of data (e.g., statistical analysis, biostatistics, computational
635 analysis):** M Viitala, R Virtakoivu, S Tadayon, J Rannikko, M Hollmén

636 **Writing, review, and/or revision of the manuscript:** M Viitala, R Virtakoivu, S Jalkanen,
637 M Hollmén

638 **Administrative, technical, or material support (i.e., reporting or organizing data,
639 constructing databases):** M Viitala, R Virtakoivu, M Hollmén

640 **Study supervision:** M Hollmén

641

642 **Acknowledgements**

643 We thank M Parsama, S Mäki, T Kanasuo and R Sjöroos for excellent technical assistance.
644 We thank the Cell Imaging Core at the Turku Centre for Biotechnology and the Central
645 Animal Laboratory at the University of Turku for their expertise and service. This study was
646 financially supported by the Sigrid Jusélius Foundation (M Hollmén), the Finnish Academy
647 (M Hollmén and S Jalkanen), the Finnish Cancer Foundation (S Jalkanen), and the Finnish
648 Cultural Foundation (R Virtakoivu).

649

650

651

652 **References**

- 653 1. Zou W, Wolchok JD, Chen L. PD-L1 (B7-H1) and PD-1 pathway blockade for cancer
654 therapy: Mechanisms, response biomarkers, and combinations. *Sci Transl Med*
655 **2016**;8:328rv4-rv4
- 656 2. Chen Daniel S, Mellman I. Oncology meets immunology: the cancer–immunity cycle.
657 *Immunity* **2013**;39:1-10
- 658 3. Gajewski TF, Schreiber H, Fu Y-X. Innate and adaptive immune cells in the tumor
659 microenvironment. *Nat Immunol* **2013**;14:1014-22
- 660 4. Chen DS, Mellman I. Elements of cancer immunity and the cancer–immune set point.
661 *Nature* **2017**;541:321-30
- 662 5. Sharma P, Hu-Lieskovan S, Wargo JA, Ribas A. Primary, adaptive, and acquired
663 resistance to cancer immunotherapy. *Cell* **2017**;168:707-23
- 664 6. Mantovani A, Marchesi F, Malesci A, Laghi L, Allavena P. Tumour-associated
665 macrophages as treatment targets in oncology. *Nat Rev Clin Oncol* **2017**;14:399-416
- 666 7. Kzhyshkowska J, Gratchev A, Goerdts S. Stabilin-1, a homeostatic scavenger receptor
667 with multiple functions. *J Cell Mol Med* **2006**;10:635-49
- 668 8. Ammar A, Mohammed RA, Salmi M, Pepper M, Paish EC, Ellis IO, *et al.* Lymphatic
669 expression of CLEVER-1 in breast cancer and its relationship with lymph node
670 metastasis. *Anal Cell Pathol (Amst)* **2011**;34:67-78
- 671 9. Algars A, Irjala H, Vaittinen S, Huhtinen H, Sundström J, Salmi M, *et al.* Type and
672 location of tumor-infiltrating macrophages and lymphatic vessels predict survival of
673 colorectal cancer patients. *Int J Cancer* **2012**;131:864-73
- 674 10. Karikoski M, Marttila-Ichihara F, Elima K, Rantakari P, Hollmen M, Kelkka T, *et al.*
675 Clever-1/stabilin-1 controls cancer growth and metastasis. *Clin Cancer Res*
676 **2014**;20:6452-64
- 677 11. Palani S, Elima K, Ekholm E, Jalkanen S, Salmi M. Monocyte Stabilin-1 Suppresses
678 the Activation of Th1 Lymphocytes. *J Immunol* **2016**;196:115-23
- 679 12. Irjala H, Alanen K, Grenman R, Heikkilä P, Joensuu H, Jalkanen S. Mannose receptor
680 (MR) and common lymphatic endothelial and vascular endothelial receptor
681 (CLEVER)-1 direct the binding of cancer cells to the lymph vessel endothelium.
682 *Cancer Res* **2003**;63:4671-6
- 683 13. Kzhyshkowska J, Gratchev A, Schmutzmaier C, Brundiers H, Krusell L, Mamidi S,
684 *et al.* Alternatively activated macrophages regulate extracellular levels of the hormone
685 placental lactogen via receptor-mediated uptake and transcytosis. *J Immunol*
686 **2008**;180:3028-37
- 687 14. Karikoski M, Irjala H, Maksimow M, Miiluniemi M, Granfors K, Hernesniemi S, *et*
688 *al.* Clever-1/Stabilin-1 regulates lymphocyte migration within lymphatics and
689 leukocyte entrance to sites of inflammation. *Eur J Immunol* **2009**;39:3477-87
- 690 15. Park SY, Jung MY, Lee SJ, Kang KB, Gratchev A, Riabov V, *et al.* Stabilin-1
691 mediates phosphatidylserine-dependent clearance of cell corpses in alternatively
692 activated macrophages. *J Cell Sci* **2009**;122:3365-73
- 693 16. Shetty S, Weston CJ, Oo YH, Westerlund N, Stamataki Z, Youster J, *et al.* Common
694 lymphatic endothelial and vascular endothelial receptor-1 mediates the transmigration
695 of regulatory T cells across human hepatic sinusoidal endothelium. *J Immunol*
696 **2011**;186:4147-55
- 697 17. Riabov V, Yin S, Song B, Avdic A, Schledzewski K, Ovsy I, *et al.* Stabilin-1 is
698 expressed in human breast cancer and supports tumor growth in mammary
699 adenocarcinoma mouse model. *Oncotarget* **2016**;7:31097-110

- 700 18. Palani S, Maksimow M, Miiluniemi M, Auvinen K, Jalkanen S, Salmi M. Stabilin-
701 1/CLEVER-1, a type 2 macrophage marker, is an adhesion and scavenging molecule
702 on human placental macrophages. *Eur J Immunol* **2011**;41:2052-63
- 703 19. Rantakari P, Patten DA, Valtonen J, Karikoski M, Gerke H, Dawes H, *et al.* Stabilin-1
704 expression defines a subset of macrophages that mediate tissue homeostasis and
705 prevent fibrosis in chronic liver injury. *Proc Natl Acad Sci* **2016**;113:9298-303
- 706 20. Schledzewski K, Falkowski M, Moldenhauer G, Metharom P, Kzhyshkowska J,
707 Ganss R, *et al.* Lymphatic endothelium-specific hyaluronan receptor LYVE-1 is
708 expressed by stabilin-1+, F4/80+, CD11b+ macrophages in malignant tumours and
709 wound healing tissue in vivo and in bone marrow cultures in vitro: implications for
710 the assessment of lymphangiogenesis. *J Pathol* **2006**;209:67-77
- 711 21. Shojaei F, Wu X, Qu X, Kowanetz M, Yu L, Tan M, *et al.* G-CSF-initiated myeloid
712 cell mobilization and angiogenesis mediate tumor refractoriness to anti-VEGF therapy
713 in mouse models. *PNAS* **2009**;106:6742-47
- 714 22. Mittal R, Chen CW, Lyons JD, Margoles LM, Liang Z, Coopersmith CM, *et al.*
715 Murine lung cancer induces generalized T cell exhaustion. *J Surg Res* **2015**;195:541-9
- 716 23. Woo SR, Turnis ME, Goldberg MV, Bankoti J, Selby M, Nirschl CJ, *et al.* Immune
717 inhibitory molecules LAG-3 and PD-1 synergistically regulate T cell function to
718 promote tumoral immune escape. *Cancer Res* **2012**;72:917-27
- 719 24. Kelly B, O'Neill LA. Metabolic reprogramming in macrophages and dendritic cells in
720 innate immunity. *Cell Res* **2015**;25:771-84
- 721 25. Byles V, Covarrubias AJ, Ben-Sahra I, Lamming DW, Sabatini DM, Manning BD, *et al.*
722 The TSC-mTOR pathway regulates macrophage polarization. *Nat Commun*
723 **2013**;4:2834
- 724 26. Chen S, Lee LF, Fisher TS, Jessen B, Elliott M, Evering W, *et al.* Combination of 4-
725 1BB agonist and PD-1 antagonist promotes antitumor effector/memory CD8 T cells in
726 a poorly immunogenic tumor model. *Cancer Immunol Res* **2015**;3:149-60
- 727 27. Lechner MG, Karimi SS, Barry-Holson K, Angell TE, Murphy KA, Church CH, *et al.*
728 Immunogenicity of murine solid tumor models as a defining feature of in vivo
729 behavior and response to immunotherapy. *J Immunother* **2013**;36:477-89
- 730 28. Fridlender ZG, Jassar A, Mishalian I, Wang L-C, Kapoor V, Cheng G, *et al.* Using
731 macrophage activation to augment immunotherapy of established tumours. *Br J*
732 *Cancer* **2013**;108:1288
- 733 29. Van der Sluis TC, Sluijter M, van Duikeren S, West BL, Melief CJM, Arens R, *et al.*
734 Therapeutic peptide vaccine-induced CD8 T cells strongly modulate intratumoral
735 macrophages required for tumor regression. *Cancer Immunol Res* **2015**;3:1042-51
- 736 30. Advani R, Flinn I, Popplewell L, Forero A, Bartlett NL, Ghosh N, *et al.* CD47
737 Blockade by Hu5F9-G4 and Rituximab in Non-Hodgkin's Lymphoma. *N Engl J Med*
738 **2018**;379:1711-21
- 739 31. Mantovani A, Longo DL. Macrophage Checkpoint Blockade in Cancer - Back to the
740 Future. *N Engl J Med* **2018**;379:1777-9
- 741 32. Broz ML, Binnewies M, Boldajipour B, Nelson AE, Pollack JL, Erle DJ, *et al.*
742 Dissecting the tumor myeloid compartment reveals rare activating antigen-presenting
743 cells critical for T cell immunity. *Cancer Cell* **2014**;26:638-52
- 744 33. Roberts EW, Broz ML, Binnewies M, Headley MB, Nelson AE, Wolf DM, *et al.*
745 Critical role for CD103+/CD141+ dendritic cells bearing CCR7 for tumor antigen
746 trafficking and priming of T cell immunity in melanoma. *Cancer Cell* **2017**;30:324-36
- 747 34. Spranger S, Dai D, Horton B, Gajewski TF. Tumor-residing Batf3 dendritic cells are
748 required for effector T cell trafficking and adoptive T cell therapy. *Cancer Cell*
749 **2017**;31:711-23

- 750 35. Pozzi L-AM, Maciaszek JW, Rock KL. Both dendritic cells and macrophages can
751 stimulate naïve CD8+ T cells in vivo to proliferate, develop effector function, and
752 differentiate into memory cells. *The Journal of Immunology* **2005**;175:2071-81
- 753 36. Kusmartsev S, Gabrilovich DI. STAT1 signaling regulates tumor-associated
754 macrophage-mediated T cell deletion. *J Immunol* **2005**;174:4880-91
- 755 37. Hamilton MJ, Bosiljcic M, LePard NE, Halvorsen EC, Ho VW, Banáth JP, *et al.*
756 Macrophages are more potent immune suppressors ex vivo than immature myeloid-
757 derived suppressor cells induced by metastatic murine mammary carcinomas. *J*
758 *Immunol* **2014**;192:512-22
- 759 38. Saio M, Radoja S, Marino M, Frey AB. Tumor-infiltrating macrophages induce
760 apoptosis in activated CD8+ T cells by a mechanism requiring cell contact and
761 mediated by both the cell-associated form of TNF and nitric oxide. *The Journal of*
762 *Immunology* **2001**;167:5583-93
- 763 39. Peranzoni E, Lemoine J, Vimeux L, Feuillet V, Barrin S, Kantari-Mimoun C, *et al.*
764 Macrophages impede CD8+ T cells from reaching tumor cells and limit the efficacy
765 of anti-PD-1 treatment. *Proc Natl Acad Sci* **2018**;115:E4041-E50
- 766 40. DeNardo DG, Brennan DJ, Rexhepaj E, Ruffell B, Shiao SL, Madden SF, *et al.*
767 Leukocyte complexity predicts breast cancer survival and functionally regulates
768 response to chemotherapy. *Cancer Discov* **2011**;1:54-67
- 769 41. Mok S, Koya RC, Tsui C, Xu J, Robert L, Wu L, *et al.* Inhibition of CSF-1 receptor
770 improves the antitumor efficacy of adoptive cell transfer immunotherapy. *Cancer Res*
771 **2014**;74:153-61
- 772 42. Zhu Y, Knolhoff BL, Meyer MA, Nywening TM, West BL, Luo J, *et al.*
773 CSF1/CSF1R blockade reprograms tumor-infiltrating macrophages and improves
774 response to T cell checkpoint immunotherapy in pancreatic cancer models. *Cancer*
775 *Res* **2014**;74:5057-69
- 776 43. Cannarile MA, Weisser M, Jacob W, Jegg A-M, Ries CH, Rüttinger D. Colony-
777 stimulating factor 1 receptor (CSF1R) inhibitors in cancer therapy. *Journal for*
778 *ImmunoTherapy of Cancer* **2017**;5:53
- 779 44. Lum HD, Buhtoiarov IN, Schmidt BE, Berke G, Paulnock DM, Sondel PM, *et al.*
780 Tumoristatic effects of anti-CD40 mAb-activated macrophages involve nitric oxide
781 and tumour necrosis factor- α . *Immunology* **2006**;118:261-70
- 782 45. Georgoudaki AM, Prokopec KE, Boura VF, Hellqvist E, Sohn S, Ostling J, *et al.*
783 Reprogramming tumor-associated macrophages by antibody targeting inhibits cancer
784 progression and metastasis. *Cell Rep* **2016**;15:2000-11
- 785 46. Kaneda MM, Messer KS, Ralainirina N, Li H, Leem CJ, Gorjestani S, *et al.* PI3K γ is
786 a molecular switch that controls immune suppression. *Nature* **2016**;539:437
- 787 47. Kanemaru H, Yamane F, Fukushima K, Matsuki T, Kawasaki T, Ebina I, *et al.*
788 Antitumor effect of Batf2 through IL-12p40 up-regulation in tumor-associated
789 macrophages. *Proc Nat Acad Scie* **2017**;114:7331-40
- 790 48. Burgdorf S, Lukacs-Kornek V, Kurts C. The mannose receptor mediates uptake of
791 soluble but not of cell-associated antigen for cross-presentation. *J Immunol*
792 **2006**;176:6770-6
- 793 49. Burgdorf S, Kautz A, Böhnert V, Knolle PA, Kurts C. Distinct Ppathways of antigen
794 uptake and intracellular routing in CD4+ and CD8+ T cell activation. *Science*
795 **2007**;316:612-6
- 796 50. Biswas SK, Allavena P, Mantovani A. Tumor-associated macrophages: functional
797 diversity, clinical significance, and open questions. *Semin Immunopathol*
798 **2013**;35:585-600

- 799 51. Bekkering S, Blok BA, Joosten LA, Riksen NP, van Crevel R, Netea MG. In Vitro
800 Experimental Model of Trained Innate Immunity in Human Primary Monocytes. Clin
801 Vaccine Immunol **2016**;23:926-33
- 802 52. Nagaraj S, Gupta K, Pisarev V, Kinarsky L, Sherman S, Kang L, *et al.* Altered
803 recognition of antigen is a mechanism of CD8+ T cell tolerance in cancer. Nature
804 Medicine **2007**;13:828
- 805 53. Lu T, Ramakrishnan R, Altiok S, Youn J-I, Cheng P, Celis E, *et al.* Tumor-infiltrating
806 myeloid cells induce tumor cell resistance to cytotoxic T cells in mice. The Journal of
807 Clinical Investigation **2011**;121:4015-29
- 808 54. Lu G, Zhang R, Geng S, Peng L, Jayaraman P, Chen C, *et al.* Myeloid cell-derived
809 inducible nitric oxide synthase suppresses M1 macrophage polarization. Nat Comm
810 **2015**;6:6676
- 811 55. Kzhyshkowska J, Gratchev A, Martens JH, Pervushina O, Mamidi S, Johansson S, *et*
812 *al.* Stabilin-1 localizes to endosomes and the trans-Golgi network in human
813 macrophages and interacts with GGA adaptors. J Leukoc Biol **2004**;76:1151-61
- 814 56. Jovanovic M, Rooney MS, Mertins P, Przybylski D, Chevrier N, Satija R, *et al.*
815 Immunogenetics. Dynamic profiling of the protein life cycle in response to pathogens.
816 Science **2015**;347:1259038
- 817 57. Irjala H, Elima K, Johansson EL, Merinen M, Kontula K, Alanen K, *et al.* The same
818 endothelial receptor controls lymphocyte traffic both in vascular and lymphatic
819 vessels. Eur J Immunol **2003**;33:815-24
- 820 58. Qian H, Johansson S, McCourt P, Smedsrod B, Ekblom M. Stabilins are expressed in
821 bone marrow sinusoidal endothelial cells and mediate scavenging and cell adhesive
822 functions. Biochem Biophys Res Commun **2009**;390:883-6
- 823 59. Boström MM, Irjala H, Mirtti T, Taimen P, Kauko T, Algars A, *et al.* Tumor-
824 associated macrophages provide significant prognostic information in urothelial
825 bladder cancer. PLoS One **2015**;10:e0133552
- 826 60. Kleinovink JW, Marijt KA, Schoonderwoerd MJA, van Hall T, Ossendorp F, Fransen
827 MF. PD-L1 expression on malignant cells is no prerequisite for checkpoint therapy.
828 Oncoimmunology **2017**;6:e1294299

829

830

831 **Figure Legends**

832

833 **Figure 1. Macrophagic Clever-1 deficiency significantly impairs the progression of solid**

834 **tumors. A**, outgrowth of subcutaneous LLC1 tumors in syngeneic wildtype, Clever-1^{-/-} and

835 *Lyz2-Cre/Clever-1^{fl/fl}* mice. **B**, representative hematoxylin/eosin-stained sections from LLC1

836 tumors collected on day 15. The dotted line demarcates the tumor mass and subcutaneous fat.

837 Scale bar, 1 mm. **C**, tumor weights, *n* = 10 per group. **D**, serum concentrations of G-CSF in

838 tumor-bearing mice, *n* = 10 per group. The data are combined from two independent

839 experiments. **E**, numbers of non-hematopoietic tumor cells (pre-gated on live CD45⁻ cells)

840 per mg of tumor, *n* = 8 mice per group. The data in **A**, **C** and **E** are combined from three

841 independent experiments. **F**, representative histograms and frequencies of PD-L1⁺ non-

842 hematopoietic tumor cells, *n* = 5 per group. Grey, IgG control; black, wildtype; blue, Clever-

843 1^{-/-}; red, *Lyz2-Cre/Clever-1^{fl/fl}*. **G**, outgrowth of orthotopic E0771 tumors in syngeneic

844 female wildtype, Clever-1^{-/-} and *Lyz2-Cre/Clever-1^{fl/fl}* mice, *n* = 5 per group. **H**, outgrowth

845 of subcutaneous EL4 tumors in syngeneic wildtype, Clever-1^{-/-}, *Tie2-Cre/ Clever-1^{fl/fl}* and

846 *Lyz2-Cre/ Clever-1^{fl/fl}* mice, *n* = 5 per group. * *P* < 0.05, ** *P* < 0.01, *** *P* < 0.001.

847

848 **Figure 2. Clever-1-deficient mice can overcome cancer-associated immunosuppression.**

849 **A** and **B**, serum concentrations of the cytokines IL-1β, IL-2, IL-12p70 and TNF-α (**A**) and the

850 chemokines CCL3, CCL4 and CCL5 (**B**) in mice bearing LLC1 tumors on day 15, *n* = 10 per

851 group. The data are combined from two independent experiments. **C**, representative

852 immunofluorescence images showing tumor T cell infiltration on day 8. Grey, CD3; blue,

853 Hoechst stain. Scale bar, 100 μm. **D**, representative dot plots and the number of T_{reg} (CD4⁺

854 CD8⁻ FoxP3⁺), CD4⁺ (CD4⁺ CD8⁻ FoxP3⁻) and CD8⁺ T cells (CD4⁻ CD8⁺ FoxP3⁻) (pre-

855 gated on live CD45⁺ CD3⁺ cells) per mg of tumor on day 15. Statistical significances between

856 CD8⁺ T cells are shown; differences between other groups were not significant. **E**, ratios of

857 CD4⁺ to CD8⁺ T cells in tumors. The data in **D** and **E** are combined from three independent

858 experiments, *n* = 10 per group. **F**, representative dot plots and frequencies of Lag3⁺ PD-1⁺

859 CD8⁺ T cells (pre-gated on live CD45⁺ CD3⁺ CD8⁺ cells) as percent of total tumor-

860 infiltrating CD8⁺ T cells, *n* = 5 per group. **G**, representative dot plots and frequencies of

861 proliferating CD8⁺ effector T cells (CD8⁺ Ki67⁺ CD44^{high} CD62L^{low}) (pre-gated on live

862 CD45⁺ CD3⁺ CD8⁺ cells) in the tumor-draining lymph nodes of mice bearing LLC1 tumors, *n*

863 = 5 per group. * *P* < 0.05, ** *P* < 0.01, *** *P* < 0.001.

864

865 **Figure 3. Macrophages and CD8⁺ T cells are essential for tumor control in Clever-1-**
866 **deficient mice. A,** schematic study design for generating bone marrow chimeras by
867 reconstituting lethally irradiated wildtype mice with bone marrow from DsRed or
868 DsRed/Clever-1^{-/-} mice and subsequent LLC1 cell injection. **B,** outgrowth of LLC1 tumors
869 in wildtype→wildtype and Clever-1^{-/-}→wildtype chimeras, *n* = 8 per group. **C,**
870 representative immunofluorescence images showing T cell infiltration (*top row*) and TAMs
871 and Clever-1 expression (*bottom row*) in LLC1 tumors on day 15. Top row: Grey, CD3; blue,
872 Hoechst stain. Bottom row: Red, F4/80; green, Clever-1; blue, Hoechst stain. Scale bar,
873 100 μm. **D,** frequencies of CD8⁺ T cells (pre-gated on live CD45⁺ CD3⁺ cells) as percent of
874 total CD3⁺ T cells, *n* = 4 mice per group. **E–G,** frequencies of TAMs (gated on live CD11b⁺
875 Ly6C^{low} Ly6G⁻ MHC II⁺ cells) as percent of total cells (**E**) and Clever-1⁺ TAMs (**F**) and
876 MHC II^{high} TAMs (**G**) as percent of total TAMs, *n* = 4 per group. **H,** relative CD206
877 expression by TAMs, *n* = 4 per group. **I,** schematic study design for depleting macrophages
878 or CD8⁺ T cells from wildtype and *Lyz2-Cre/Clever-1^{fl/fl}* mice with anti-CD115 and anti-
879 CD8β antibodies, respectively, before LLC1 cell injection. **J,** outgrowth of subcutaneous
880 LLC1 tumors in wildtype and *Lyz2-Cre/Clever-1^{fl/fl}* mice treated with IgG, anti-CD115 or
881 CD8β antibodies. **K,** remaining TAMs (*left*) (gated on live CD45⁺ CD3⁻ CD8⁻ CD11b⁺
882 Ly6C^{low} Gr-1⁻ cells) and CD8⁺ T cells (*right*) (gated on live CD45⁺ CD3⁺ CD8⁺ CD11b⁻
883 cells) as percent of irrelevant IgG treatment. **J** and **K,** *n* = 4 per group. * *P* < 0.05, *** *P* <
884 0.001.

885

886 **Figure 4. Tumor-associated macrophages acquire an immunostimulatory phenotype in**
887 **the absence of Clever-1. A,** representative immunofluorescence images showing Clever-1
888 expression by TAMs (*top row*) and tumor endothelial cells (*bottom row*) in LLC1 tumors
889 collected on day 8. Top row: red, F4/80; green, Clever-1; blue, Hoechst stain. Bottom row:
890 red, CD31; green, Clever-1. Scale bar, 100 μm. **B,** representative dot plots and amounts of
891 TAMs (Ly6C^{low} Ly6G⁻ MHC II⁺), M-MDSCs (Ly6C^{high} Ly6G⁻) and PMN-MDSCs
892 (Ly6C^{intermediate} Ly6G⁺) (pre-gated on live CD11b⁺ cells) per mg of tumor on day 15.
893 Statistical significances between TAMs are shown; differences between other groups were
894 not significant. **C,** relative Ki67 expression by M-MDSCs in tumors grown in wildtype and
895 Clever-1^{-/-} mice, *n* = 5 per group. **D,** representative dot plots and frequencies of MHC II^{high}
896 TAMs as percent of total TAMs. **E,** relative CD206 expression by MHC II^{high} TAMs. The
897 data in **B–E** are combined from three independent experiments, *n* = 10 per group. **F,**
898 frequencies of PD-L1⁺ TAMs as percent of total TAMs, *n* = 5 per group. **G,** representative

899 histograms and quantification of Nos2 induction in TAMs treated overnight with LPS, $n = 5$
900 per group. Grey, IgG control; blue, - LPS; red, + LPS. **H**, concentration of IL-12p40 in
901 tumor lysates, $n = 8$ per group. **I**, concentration of secreted IL-12p40 in supernatants of
902 TAMs isolated from tumors and stimulated with LPS overnight, $n = 4$ per group. * $P < 0.05$,
903 ** $P < 0.01$, *** $P < 0.001$.

904

905 **Figure 5. Elevated mTOR signaling in Clever-1-deficient macrophages associates with**
906 **an increasingly inflammatory phenotype. A**, glycolysis stress test on TAMs enriched from
907 LLC1 tumors on day 15. Glucose (gluc), oligomycin (oligo) and 2-deoxyglucose (2-DG)
908 were added at the indicated time points. ECAR, extracellular acidification rate. **B**, quantified
909 glycolysis (*left*) and glycolytic capacity (*right*) in TAMs. **A** and **B**, $n = 4$ per group. **C**,
910 frequencies of CD206⁺ MHC II⁺, CD206⁺ MHC II⁻ and CD206⁻ MHC II⁻ wildtype and
911 Clever-1^{-/-} BMDMs after polarization with dexamethasone. **D**, relative PD-L1 expression by
912 dexamethasone-polarized wildtype and Clever-1^{-/-} BMDMs. **E**, IL-10 secretion by
913 dexamethasone-polarized wildtype and Clever-1^{-/-} BMDMs after LPS stimulation. **C-E**, $n =$
914 4 per group. **F** and **G**, metabolic phenotype test showing glycolysis (**F**) and oxidative
915 phosphorylation (**G**) on dexamethasone-polarized wildtype and Clever-1^{-/-} BMDMs at
916 baseline and after LPS stimulation overnight (+ LPS). Oligomycin (oligo) and FCCP were
917 added at the indicated time points. OCR, oxygen consumption rate. **H**, Relative Clever-1
918 mRNA expression in dexamethasone-polarized wildtype BMDMs after LPS stimulation, $n =$
919 3. **I**, representative western blots showing mTOR and NF- κ B phosphorylation after LPS
920 stimulation in dexamethasone-polarized wildtype and Clever-1^{-/-} BMDMs. GAPDH serves
921 as the loading control. The experiment was repeated five times with similar results. **J**, band
922 quantification of mTOR (*left*) and NF- κ B (*right*) phosphorylation in **I** normalized to GAPDH.
923 **K**, relative mTOR phosphorylation in dexamethasone-polarized wildtype and Clever-1^{-/-}
924 BMDMs after LPS stimulation analyzed by flow cytometry, $n = 4$ per group. * $P < 0.05$, ** P
925 < 0.01 .

926

927 **Figure 6. Immunotherapeutic Clever-1 blockade significantly limits tumor growth and**
928 **reactivates the antitumor CD8⁺ T cell response. A**, schematic study design for treating
929 tumor-bearing wildtype mice with antibodies against Clever-1, PD-1 or combination thereof.
930 **B**, photograph of tumors collected on day 15. **C**, outgrowth of LLC1 tumors in wildtype mice
931 treated as indicated in **A**. **D**, tumor weights. **E**, numbers of non-hematopoietic tumor cells
932 (gated on live CD45⁻ cells) per mg of tumor. **F**, frequencies of PD-L1⁺ non-hematopoietic

933 tumor cells as percent of total non-hematopoietic tumor cells. **G**, numbers of T_{reg} (CD4⁺
934 CD8⁻ FoxP3⁺), CD4⁺ (CD4⁺ CD8⁻ FoxP3⁻) and CD8⁺ T cells (CD4⁻ CD8⁺ FoxP3⁻) (pre-
935 gated on live CD45⁺ CD3⁺ cells) per mg of tumor. Statistical significance between CD8⁺ T
936 cells is shown; other differences were not significant. **H**, frequencies of proliferating PD-1⁻
937 CD8⁺ T cells (Ki67⁺ PD-1⁻ CD8⁺) (pre-gated on live CD45⁺ CD3⁺ CD8⁺ cells) as percent of
938 total tumor-infiltrating CD8⁺ T cells. **I**, numbers of TAMs (Ly6C^{low} Ly6G⁻ MHC II⁺), M-
939 MDSCs (Ly6C^{high} Ly6G⁻) and PMN-MDSCs (Ly6C^{intermediate} Ly6G⁺) (pre-gated on live
940 CD11b⁺ cells) per mg of tumor. The shown statistical significances refer to differences
941 between TAMs and PMN-MDSCs; differences between M-MDSCs were not significant. **J**,
942 frequencies of Clever-1⁺ TAMs as percent of total TAMs. **B–J**, *n* = 5 per group. * *P* < 0.05,
943 ** *P* < 0.01, *** *P* < 0.001.

944
945

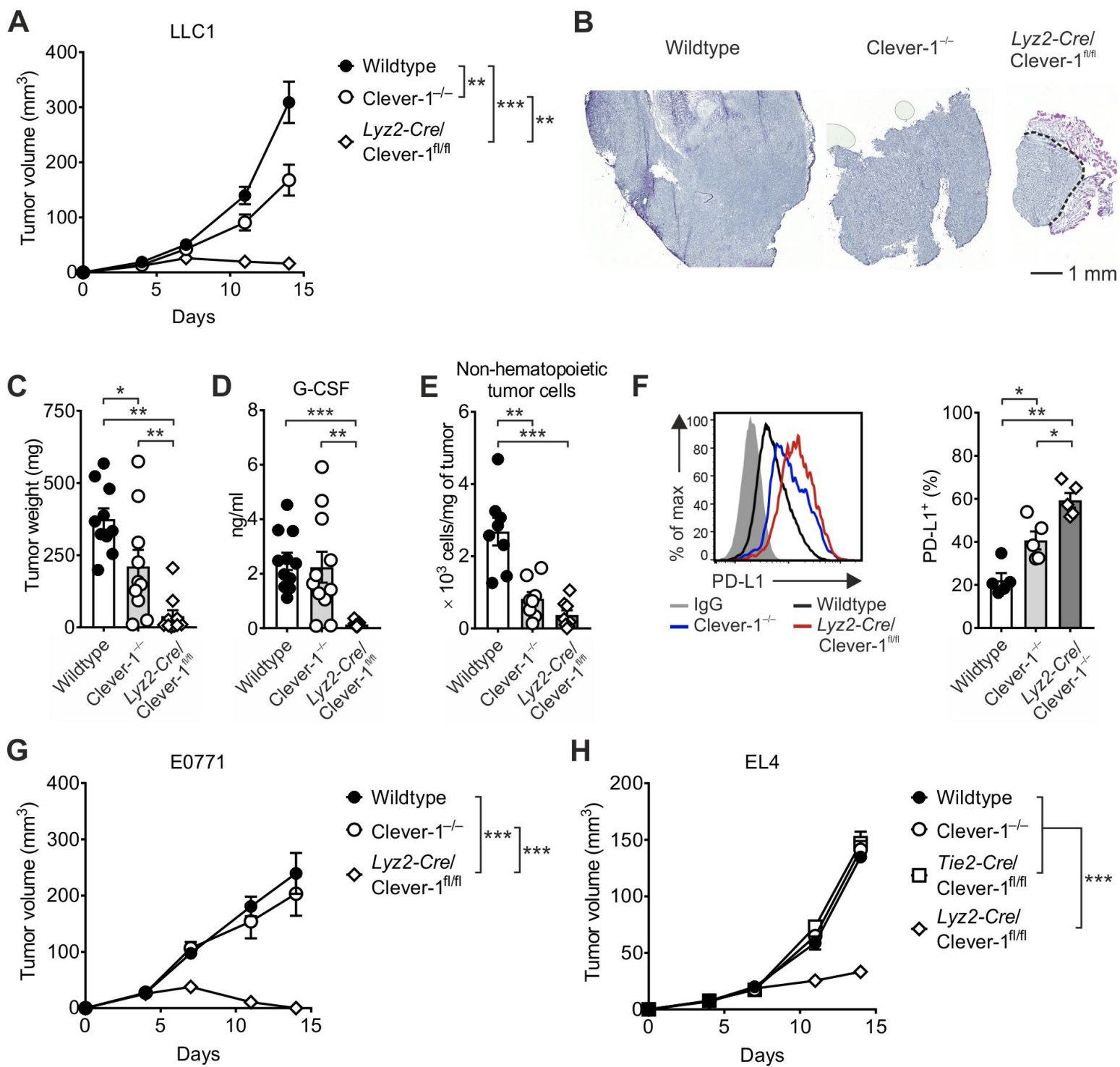


Figure 1

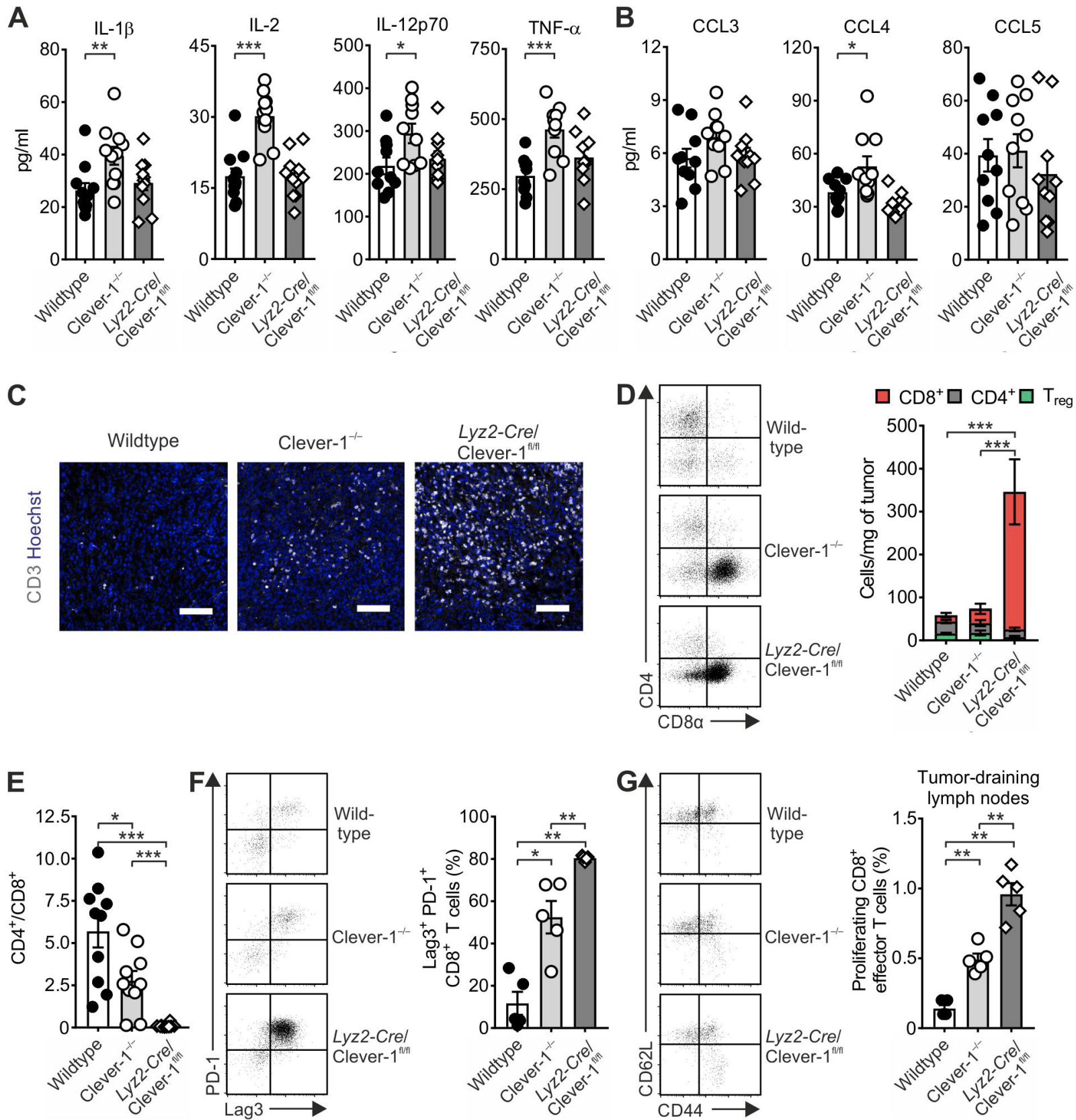


Figure 2

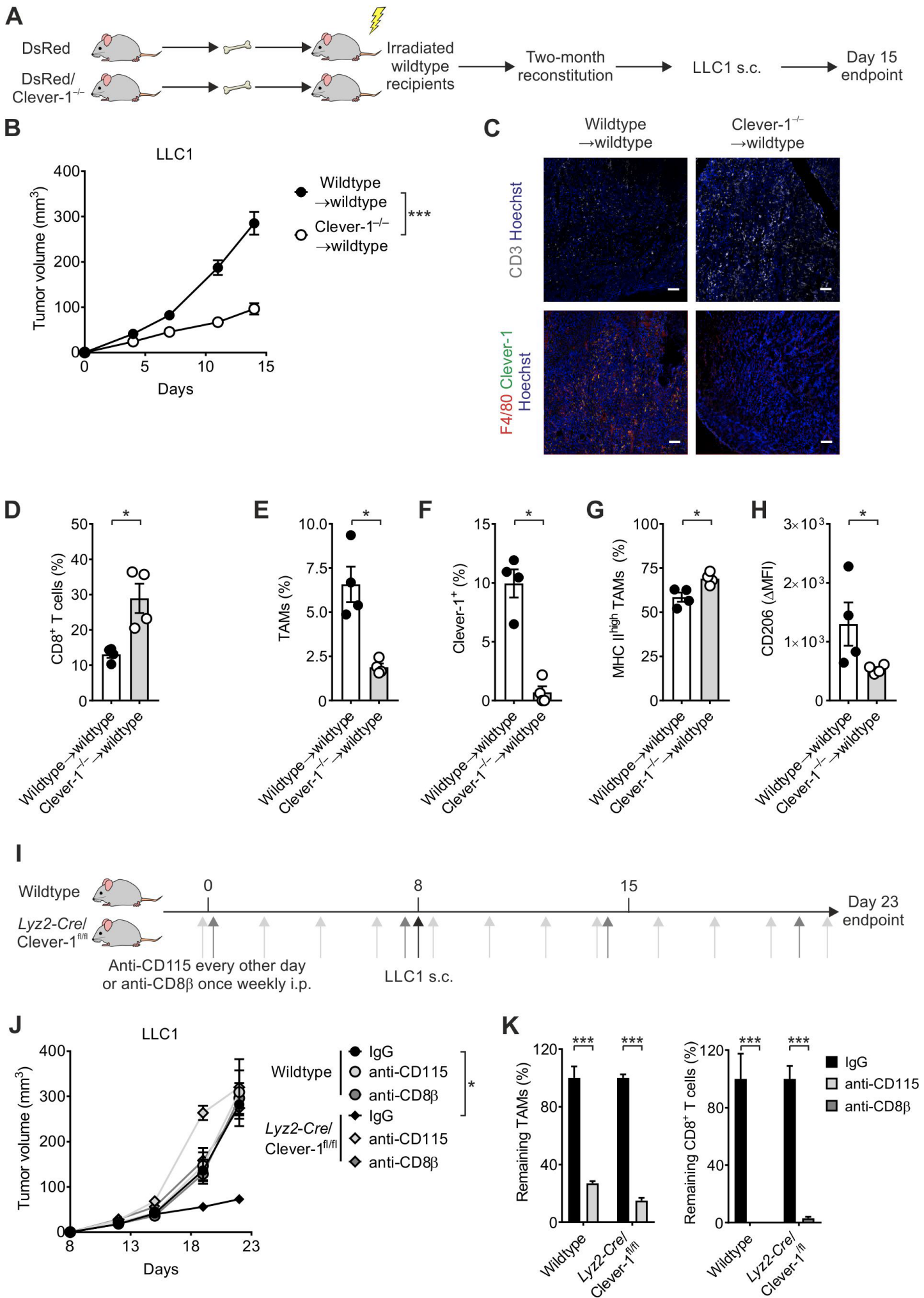


Figure 3

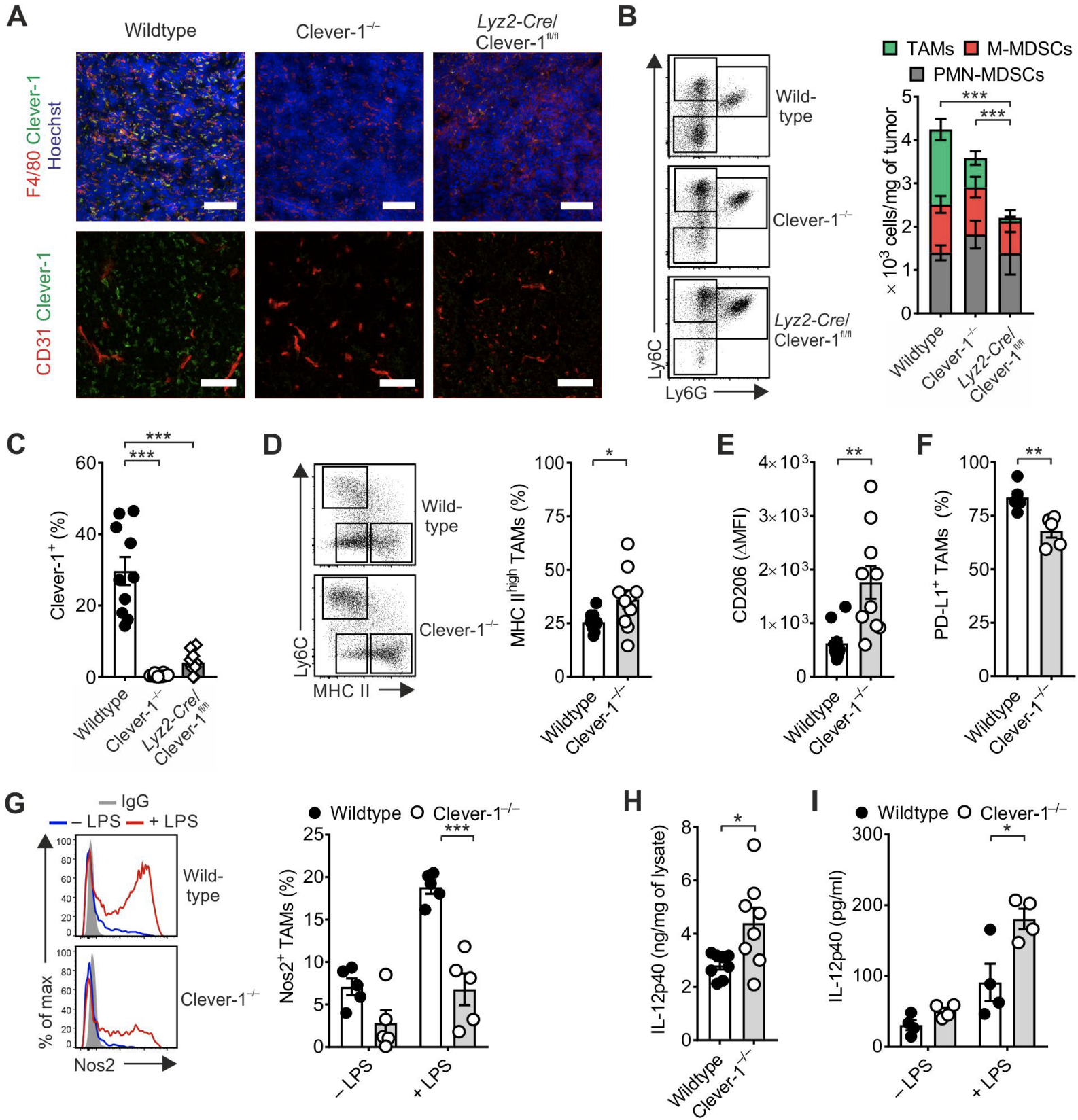


Figure 4

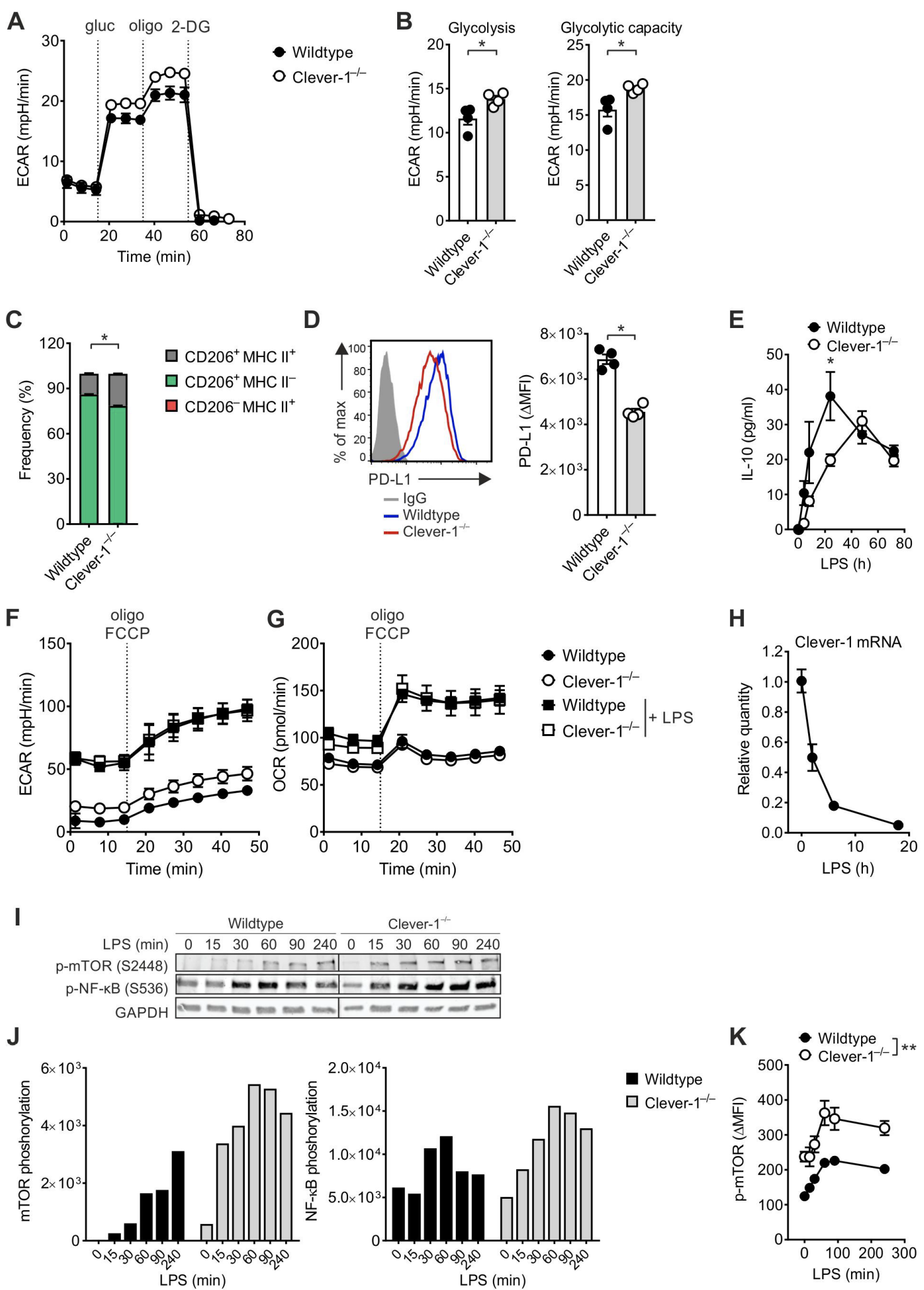


Figure 5

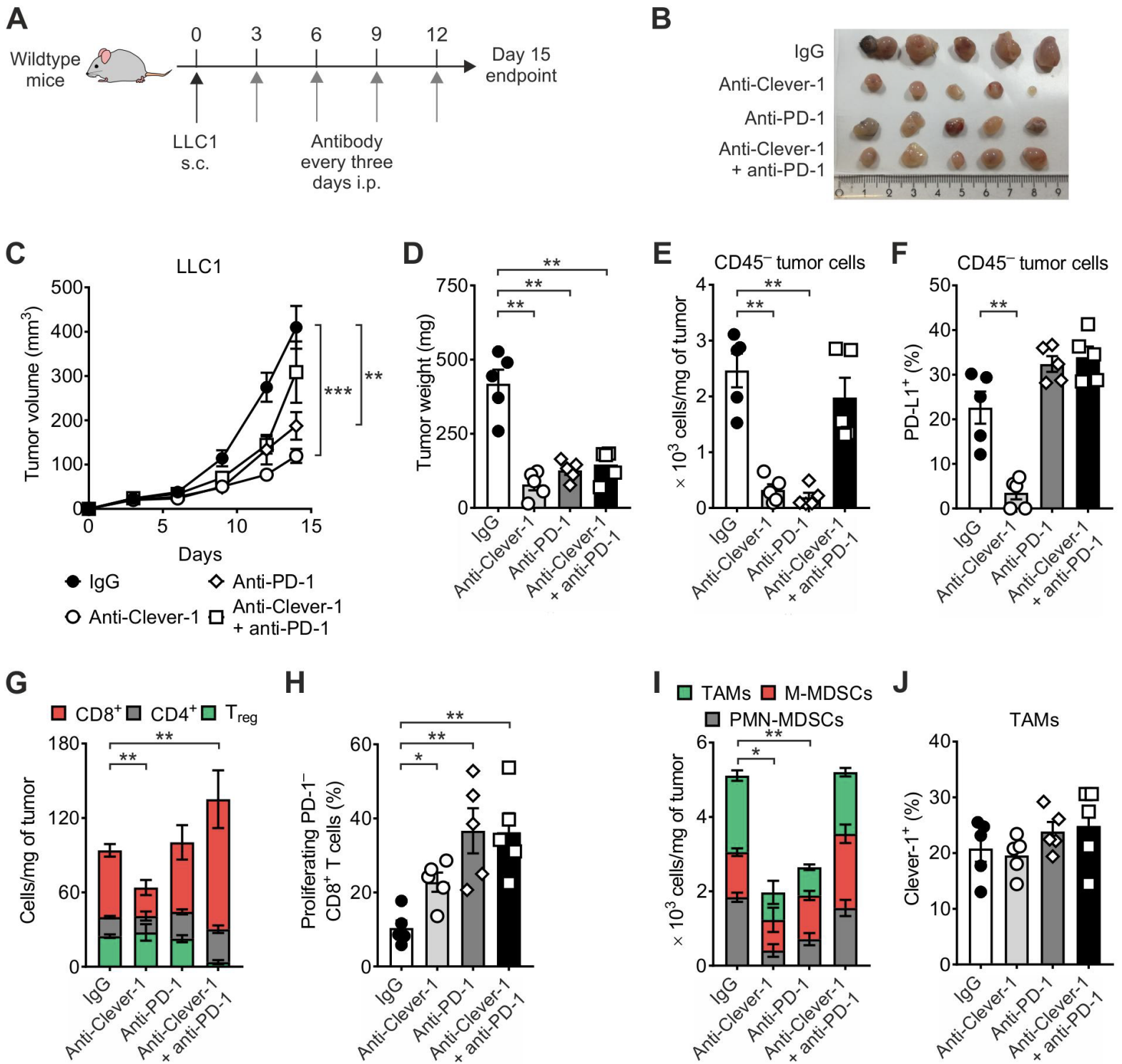


Figure 6